

# An Ancient Metal-Poor Population in M32, and Halo Satellite Accretion in M31, Identified by RR Lyrae Stars<sup>\*</sup>

Ata Sarajedini<sup>1†</sup>, S. -C. Yang<sup>1</sup>, A. Monachesi<sup>2</sup>, Tod R. Lauer<sup>3</sup>, and S. C. Trager<sup>4</sup>

<sup>1</sup>University of Florida, Department of Astronomy, 211 Bryant Space Science Center, Gainesville, FL, 32611 USA

<sup>2</sup>Department of Astronomy, University of Michigan, 830 Dennison Building, 500 Church Street, Ann Arbor, MI 48109, USA

<sup>3</sup>National Optical Astronomy Observatory, P.O. Box 26732, Tucson, AZ 85726, USA

<sup>4</sup>Kapteyn Astronomical Institute, P.O. Box 800, 9700 AV Groningen, The Netherlands

## ABSTRACT

We present time-series photometry of two fields near M32 using archival observations from the Advanced Camera for Surveys Wide Field Channel onboard the Hubble Space Telescope. One field is centered about 2 arcmin from M32 while the other is located 15 arcmin to the southeast of M31. The imaging covers a time baseline sufficient for the identification and characterization of a total number of 1139 RR Lyrae variables of which 821 are ab-type and 318 are c-type. In the field near M32, we find a radial gradient in the density of RR Lyraes relative to the center of M32. This gradient is consistent with the surface brightness profile of M32 suggesting that a significant number of the RR Lyraes in this region belong to M32. This provides further confirmation that M32 contains an ancient stellar population formed around the same time as the oldest population in M31 and the Milky Way. The RR Lyrae stars in M32 exhibit a mean metal abundance of  $\langle [\text{Fe}/\text{H}] \rangle \approx -1.42 \pm 0.02$ , which is  $\approx 15$  times lower than the metal abundance of the overall M32 stellar population. Moreover, the abundance of RR Lyrae stars normalized to the luminosity of M32 in the field analyzed further indicates that the ancient metal-poor population in M32 represents only a very minor component of this galaxy, consistent with the 1% to 4.5% in mass inferred from the CMD analysis of Monachesi et al. We also find that the measured reddening of the RR Lyrae stars is consistent with M32 containing little or no dust. In the other field, we find unprecedented evidence for two populations of RR Lyraes in M31 as shown by two distinct sequences among the ab-type variables in the Bailey Diagram. When interpreted in terms of metal abundance, one population exhibits a peak at  $[\text{Fe}/\text{H}] \approx -1.3$  and the other is at  $[\text{Fe}/\text{H}] \approx -1.9$ . One possible interpretation of this result is that the more metal-rich population represents the dominant M31 halo, while the metal-poorer group could be a disrupted dwarf satellite galaxy orbiting M31. If true, this represents a further indication that the formation of the M31 spheroid has been significantly influenced by the merger and accretion of dwarf galaxy satellites.

**Key words:** stars: variables: other – galaxies: stellar content – galaxies: spiral – galaxies: individual (M31)

## 1 INTRODUCTION

### 1.1 RR Lyraes and their use in unveiling stellar populations

The class of pulsating stars known as RR Lyrae variables are located at the intersection of the instability strip and the horizontal branch in the Hertzsprung Russell Diagram (Smith 1995). There are three principal types of RR Lyrae

variables; those pulsating in the fundamental mode exhibit sawtooth-like light curves and are referred to as ab-type or RR0 variables. The first overtone pulsators generally show sine-curve shaped light curves, have shorter periods and typically lower amplitudes than the ab-types, and are referred to as c-type or RR1 variables. Lastly, RR Lyraes that pulsate in both the fundamental and first overtone modes (i.e. double mode pulsators) carry the d-type moniker.

The astrophysical utility of RR Lyraes to investigate a number of key questions in the areas of stellar populations and galaxy formation is well documented. For example, be-

† E-mail: ata@astro.ufl.edu

cause of their low masses ( $\approx 0.7 M_{\odot}$ , Smith 1995), the mere presence of RR Lyrae stars in a stellar population suggests an old age ( $\gtrsim 10$  Gyr) for the system. As such, one does not need to obtain deep photometry beyond the old main sequence turnoff in order to establish the presence of an old population.

The periods and amplitudes of the ab-type RR Lyrae stars ( $P_{ab}$ ) are related to their metallicities. Using data on Milky Way field RR Lyraes from Layden (2005, private communication) and those in the Large Magellanic Cloud, Sarajedini et al. (2006) and Alcock et al. (2000), respectively, present relations that correlate the periods and amplitudes of RR Lyraes with their metal abundances. Once the metallicities of the RR Lyraes are determined, their absolute magnitudes can be calculated using relations between [Fe/H] and the absolute magnitude of the RR Lyraes [ $M_V(\text{RR})$ ], which is then used to estimate the distance to their parent population, be it a star cluster or a galaxy. Lastly, ab-type RR Lyraes are also useful for calculating the line-of-sight reddening. The minimum light colors of these stars are largely independent of their other properties as shown by Gulden-schuh et al. (2005) and Kunder et al. (2010) making the determination of reddening a simple one-step process.

Thus far, we have presented examples of how RR Lyrae variables can be powerful probes of the systems in which they reside - star clusters or among the field populations of galaxies. It is for this reason that studying them in Local Group galaxies like M31 and M32 provides valuable insights into the properties of these systems.

## 1.2 RR Lyrae variables in M31

The study of RR Lyraes in M31 has a rich history dating back to the seminal work of Pritchett & van den Bergh (1987) and culminating in the most recent papers by Sarajedini et al. (2009) and Jeffrey et al. (2011). Sarajedini et al. (2009, hereafter S09) present Hubble Space Telescope (HST) Advanced Camera for Surveys (ACS) observations for two fields in the range of 4 to 6 kpc from the center of M31. A total of 681 RR Lyraes (555 ab-type and 126 c-type) were identified in the two fields. A mean metal abundance of [Fe/H]  $\approx -1.5$  was determined using the periods and amplitudes of these stars.

Jeffery et al. (2011) is a continuation of the work of Brown et al. (2004) and presents high quality light curves for RR Lyraes in 5 fields around M31. These include a halo field at 21 kpc, and two halo fields at 35 kpc. In addition, there is a field coincident with one of the streams in the vicinity of M31 and one that covers a disk region about 26 kpc from the center along the major axis of the galaxy. Besides identifying a number of RR Lyrae variables in these fields, Jeffery et al. (2011) also compare three methods for the determination of RR Lyrae metallicities. We note in passing also that Bernard et al. (2012) present RR Lyraes in two M31 fields along the major axis based on HST/ACS observations. These are located in the disk warp and in the outer disk.

## 1.3 RR Lyrae variables in M32

M32 is an intriguing galaxy, considered to be the prototype of the compact elliptical galaxies. In view of its im-

portance in understanding these objects, its stellar populations have been extensively studied (e.g., Rose 1985, Freedman 1992, Grillmair et al. 1996, Worthey 2004, Trager et al. 2000, Rose et al. 2005). Recently, using the High Resolution Channel (HRC) on ACS, Monachesi et al. (2011, 2012) have analyzed the stellar populations of M32 in a field  $\sim 2'$  away from its nucleus. They have constructed the deepest optical color magnitude diagram (CMD) of M32 ever and derived its star formation history (SFH). They found that M32 has had an extended SFH and is composed of two main dominant populations: a 2–5 Gyr old, metal rich population and a population older than 5 Gyr, with slightly subsolar metallicity. Their study moreover indicates that a significant contribution from stars older than 10 Gyr is not expected, although there are claims from spectroscopic analysis that such a population should exist in M32 (e.g., Coelho et al. 2009). Given the extreme crowding in their field, Monachesi et al. (2011) were unable to detect the oldest main sequence turnoff (MSTO) of M32 and thus a census of the oldest stars in M32 is still missing. RR Lyrae stars are therefore a direct indicator of the presence of an ancient population in M32. Alonso-Garcia et al. (2004) used the Wide Field Planetary Camera 2 (WFPC2) onboard HST to image a field  $\approx 3.5$  arcmin to the east of M32. Comparing the variable star content of this field with that of a control field that samples the M31 field away from M32, they claim to have identified RR Lyraes that belong to M32, although this result remains quite uncertain, since their data suffer from strong photometric and temporal incompleteness. A marginal detection of RR Lyrae stars in M32 was presented by Fiorentino et al. (2010). They used the same HRC field of HST/ACS as Monachesi et al. (2011) and identified 17 RR Lyrae variables. Using a Bayesian analysis, they suggest that M32 contains RR Lyrae stars and therefore possesses an old ( $\gtrsim 10$  Gyr) population. However, the small field of view of ACS/HRC and the strong contamination from M31 makes this detection also very uncertain.

As we were preparing this paper, we became aware of the most recent work from Fiorentino et al. (2012), which presents their reduction and analysis of a subset of the data presented herein. They studied the RR Lyraes in the M32 field and investigated their spatial distribution as well as their periods and metallicities. We will highlight their work in more detail within the relevant sections of the present paper, but for the moment, we note that their results are largely in agreement with ours.

## 1.4 This paper

In the present work, we utilize archival wide field channel (WFC) HST/ACS images of two fields in the vicinity of M32 in order to search for RR Lyraes. The ACS/WFC fields have a wider spatial coverage of M32's stellar populations over a range of higher surface brightnesses than the previous WFPC2 and ACS/HRC fields studied. Our primary task is to identify a substantial population of RR Lyraes belonging to M32 that would confirm the presence of a truly ancient, metal-poor population in this galaxy, and characterize their properties so that we can use them to study their parent galaxy. Furthermore, we probe the RR Lyraes in the spheroid of M31 in order to better understand their properties: their metallicities and Oosterhoff types.

The paper is organized as follows. Sections 2 and 3 describe our observations and data reduction including the artificial star experiments we use to characterize our photometric incompleteness. Section 4 provides a description of the techniques used to identify and characterize the RR Lyraes in our sample. We also detail the simulations used to assess any biases present in our variability data. The results and discussion as they pertain to M32 are in Section 5, where we investigate the membership of the RR Lyraes in our field closest to M32. Section 6 presents the results and discussion of the RR Lyraes that belong to M31, where we show unprecedented evidence for two sequences of ab-type RR Lyraes in the Bailey Diagram. Finally, the conclusions of the present work are given in Section 7.

## 2 OBSERVATIONS

The observations used in the present study were obtained with HST/ACS/WFC as part of program GO-9392 (PI: Mateo). The details of this program have already been fully described by Rudenko et al. (2009) and the observing log is shown in Table 1. In summary, two fields were observed; the first one, which we designate ‘M32’ in Fig. 1, was centered southeast of M32 covering a radial distance range of 1 to 4.5 arcmin from the center of M32. Figure 2 shows a reproduction of the M32 field observed in the F606W filter. The second field was meant to be a control field (designated ‘Control’ in Fig. 1) located roughly 5 arcmin northeast of M32 in order to monitor the M31 background field in the vicinity of M32. The M32 field was observed for a total of  $\sim 5$  hours in the F606W filter and  $\sim 8$  hours in F814W alternating between the two filters and yielding 18 exposures in each filter. These were taken on 2004 November 24–25 and 2004 December 10. Similarly, the Control field was observed on 2004 December 20–22 for  $\sim 5$  and  $\sim 7.5$  hours in F606W and F814W, respectively, again alternating between filters and providing 18 exposures per filter. Figure 3 shows raw unphased light curves for two of our RR Lyrae variables in order to illustrate the cadence of the observations.

It is important to note that, as we establish below, the properties of the M31 RR Lyraes in the Control field are significantly different from those in the M32 field. As such, we did not make use of the Control field in the manner it was originally intended - to gauge the level of contamination of M32 stars by the M31 background. Instead, we have determined the background density using selected data from the M32 field as well as the observations presented by S09. Section 5.2 provides more details on the procedure we followed.

## 3 DATA REDUCTION

### 3.1 Program Frames

The 72 ACS/WFC images were measured using the DAOPHOT/ALLSTAR/ALLFRAME (Stetson 1987; 1994) suite of crowded field photometry programs. The procedure we followed is identical to that used by Sarajedini et al. (2009, hereafter S09). In summary, once a master coordinate file was constructed for each image and high precision coordinate transformations between the images established,

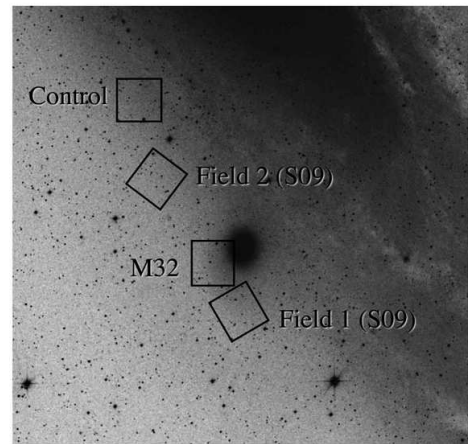


**Figure 1.** The location of our ACS fields (M32 and Control) along with the two fields from S09 overplotted on a digitized sky survey image in the region of M31. The dwarf elliptical galaxy M32 is near the center of the image. North is up and east is to the left.

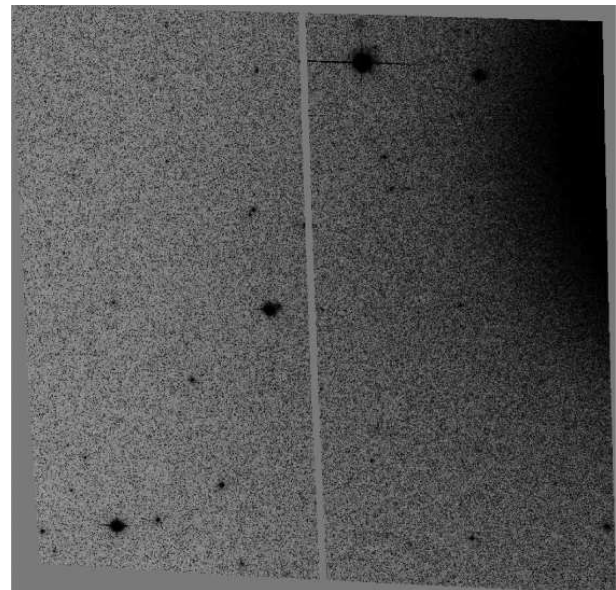


**Figure 2.** The F606W filter drizzled ACS image of our M32 field. North is up and east is to the left.

ALLFRAME was used to fit a high signal-to-noise point spread function to all detected profiles on each of the 36 images in each field. The measurements on each of the individual frames were then matched and only stars appearing on all 36 images were kept.

The standardization procedure of the individual magnitudes is identical to that used by Sarajedini et al. (2006). More specifically, we have made use of the Reiss & Mack (2004) prescription to account for the effects of charge transfer efficiency along with the Sirianni et al. (2005) calibration equations and coefficients to transform our instrumental photometry to the ground-based *VI* system. Each of our magnitude measurements is affected by three sources of systematic error: the uncertainty in the aperture corrections

**Table 1.** Observing Log.

Field	R. A. (J2000)	Dec (J2000)	Starting Date	Data Sets	Filter	Exp Time
M32	00 42 55.92	+40 50 50.4	2004 Nov 24	J8F101, J8F103, J8F105	F606W F814W	2 x 900s, 1 x 960s, 15 x 1000s 1 x 1520s, 3 x 1570s, 14 x 1580s
Control	00 43 28.65	+41 03 43.8	2004 Dec 20	J8F102, J8F104, J8F106	F606W F814W	2 x 900s, 1 x 960s, 15 x 1000s 1 x 1520s, 3 x 1570s, 14 x 1580s

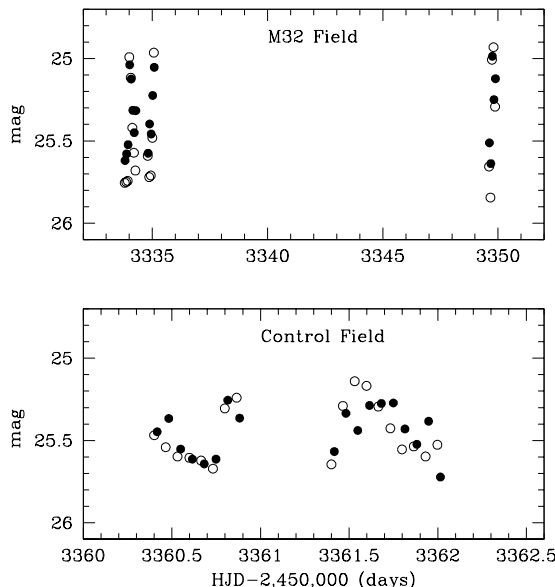


**Figure 3.** Raw unphased light curves for two of the RR Lyraes in our sample illustrating the cadence of the observations in each field. The filled circles are the F606W filter data while the open circles are in F814W.

( $\pm 0.02$  mag), the error in the correction to infinite aperture for the F606W ( $\pm 0.00$  mag) and F814W ( $\pm 0.001$  mag) filters, and the error in the ground system VI zero point ( $\pm 0.05$  mag, Sirianni et al. 2005).

### 3.2 Artificial Star Experiments

In order to gauge the degree of photometric completeness on our program frames, we have performed a series of artificial star experiments. Beginning with a synthetic color-magnitude diagram (CMD) generated using IAC-STAR (Aparicio & Gallart 2004) that replicates the appearance of the actual CMD produced from our observations, we selected 50,000 artificial stars. These were placed on the WFC2 images, which is the portion of the field closer to M32, 5,000 stars at a time, in a grid pattern with random intra-pixel positions. The WFC1 region of the field, which is less crowded than WFC2, received 35,000 artificial stars. The resultant images were photometered using the same procedure as the

original images. The overall recovery rates for the artificial stars were 87% for the WFC1 images and 81% for WFC2.

The recovery rates were used to devise a relation between completeness fraction and radial distance from the center of M32. Since we are interested in correcting the red clump stars and RR Lyrae for photometric incompleteness (see below), we limited this relation to stars in the magnitude range of the horizontal branch.

## 4 CHARACTERIZATION OF THE VARIABLE STARS AND SIMULATIONS

We use the technique of Yang et al. (2010) and Yang & Sarajedini (2012) to identify and characterize variable stars in the images. We start by searching all of the variable star candidates located in a range of  $V$  magnitude ( $24.5 < V < 26$ ). Stars within this  $V$  magnitude range were evaluated using a reduced  $\chi^2_{VI}$  defined by the following equation :

$$\chi^2_{VI} = \frac{1}{N_V + N_I} \times \left[ \sum_{i=1}^{N_V} \frac{(V_i - \bar{V})^2}{\sigma_i^2} + \sum_{i=1}^{N_I} \frac{(I_i - \bar{I})^2}{\sigma_i^2} \right]$$

Any anomalous data points that deviated from the mean magnitude by  $\pm 3\sigma$  were excluded from the  $\chi^2_{VI}$  calculation for each star. Then, we selected only those stars with  $\chi^2_{VI}$  values greater than 3.0 as potential variable candidates.

The next step involved running our template light curve fitting routine, RRFIT (Yang & Sarajedini 2011) on the time series photometry of these variable star candidates in order to detect and characterize RR Lyrae stars. RRFIT uses 25 unique light curve templates (23 RRab type and 2 RRc type variables). It searches over specific period and amplitude ranges and calculates the  $\chi^2$  difference between the observed data and each light curve template. It then determines the optimal light curve parameters such as period, amplitude, maximum epoch, and mean magnitude from the best-fit template (i.e. the template that minimizes the  $\chi^2$  value).

After applying the above technique, we have identified and characterized 509 RR Lyrae variables (375 ab-type and 134 c-type) in the M32 field and 630 RR Lyrae (446 ab-type and 184 c-type) in the Control field. By way of comparison, Fiorentino et al. (2012) found 416 RR Lyrae variables (314 ab-type and 102 c-type) in the same M32 field analyzed herein. Figure 4 shows a representative sample of our light curves. Tables 2–9 list the basic properties of each of these RR Lyrae variables.

In order to investigate the presence of any biases in our period-finding algorithm, we have performed extensive simulations wherein we produce  $\sim 1000$  synthetic RR Lyrae light

curves with a range of ab-type and c-type periods and amplitudes. We then input these raw synthetic light curves into RRFIT in order to determine their properties and compare them with their known values. The results are shown in Figs. 5 and 6, where we plot the difference between the input and output periods ( $\Delta P$ ) as a function of input period. In order to estimate the errors of the individual RR Lyrae periods, we performed the following statistical test introduced in Yang et al. (2010) and also used in Yang & Sarajedini (2012). From the artificial RR Lyrae lists, we randomly draw the same number of artificial RR Lyrae stars as the observed RR Lyraes in each field [M32 : 375 (RRab) and 134 (RRc); Control : 446 (RRab) and 184 (RRc)] to calculate an average  $\Delta P$  value for each sample drawn. We consider the spread of a  $\Delta P$  distribution as the estimate of the error. To increase its statistical significance, we iterated this sampling 10,000 times. The average spread ( $\langle \sigma \rangle$ ) of 10,000 samples provides a realistic error for our period measurements. We applied the same method to calculate errors in the  $V$ -band amplitude. The resulting values of the errors are shown in Table 10. Also displayed in this table is the fraction of simulations where the recovered period differed from the input period by less than  $\pm 0.05$  d and  $\pm 0.1$  d.

We note that the simulations reveal little or no aliasing among the RR Lyrae periods of the Control field. Even in the M32 field, where Fig. 5 does show the signature of aliasing, the number of stars in the aliased ‘bands’ is a small fraction of the total number of simulations run as demonstrated by the values in Table 10. In fact, we found no significant biases in our determination of the mean periods and amplitudes as shown by the relatively small errors listed in Table 10. Hence, we assume that period aliasing does not significantly affect the results in the remainder of our analysis, which is mainly focused on the mean periods, mean amplitudes, and results derived from them.

## 5 RR LYRAE VARIABLES IN M32

We first examine the properties of the RR Lyrae variables in M32. Figures 7 and 8 show the color-magnitude diagrams (CMDs) of the WFC1 and WFC2 chips in the M32 field. Both CMDs show a strong red giant branch (RGB), RC, asymptotic giant branch bump ( $\approx 1$  mag above the RC), and RGB bump ( $\approx 0.5$  mag below the RC). These features were first detected in the CMD presented by Monachesi et al. (2011), constructed from an ACS/HRC field which is entirely overlapped by our observations. Monachesi et al. (2011) showed that the CMD locations of those features indicate that the bulk of the stellar population in M32 at  $\sim 2'$  from its center is 8–10 Gyr old. The WFC2 CMD clearly shows more scatter, which is not unexpected given the fact that it is located closer to the center of M32. The RR Lyrae variables are also plotted in these CMDs and occupy a region that is typical for these stars.

### 5.1 The Radial Density Profile of RR Lyraes around M32

We are interested in establishing the membership of our RR Lyrae sample with regard to whether the majority of these stars belong to M32 or the background M31 population. To

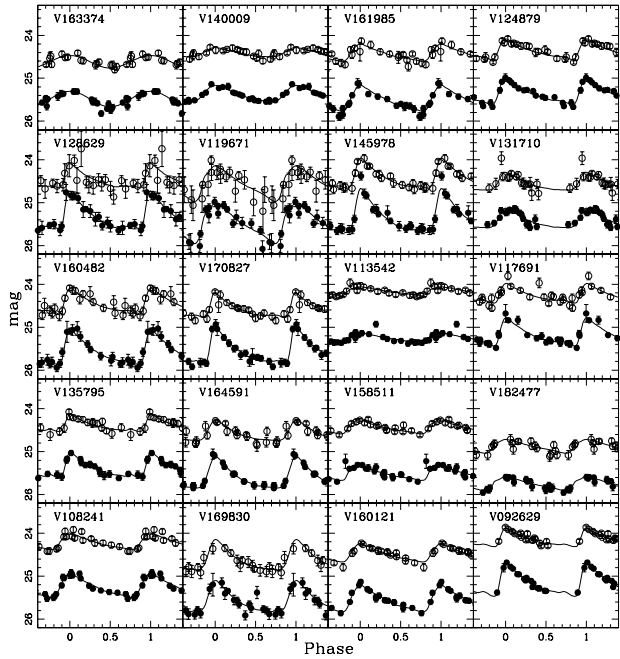


**Figure 4.** Example light curves of some of the RR Lyrae stars in our sample. The filled circles are the F606W filter data while the open circles are in F814W. The latter have been adjusted brighter by 1 mag for illustrative purposes.

do so, we show the radial density distribution of these stars projected onto the major axis of M32 as compared with the RC stars in Fig. 9. The red clump stars are core-helium burning horizontal branch stars in the same phase of evolution as the RR Lyraes. To isolate these stars, we use a  $I$ -band magnitude range of 24.2–25.2 and a color range of 0.8–1.2. The upper panel of Fig. 9 illustrates the radial density profiles of the RC and RR Lyrae stars from the present study where we have applied photometric completeness corrections based on the artificial star experiments described earlier. We also include the RR Lyraes from the F1 HRC field of Fiorentino et al. (2010, cross) and from Field 1 of S09 (open squares). The profiles of the RR Lyrae stars have been scaled to match the RC stars in the region outside of 150 arcsec. The dashed line in the upper panel of Fig. 9 is our adopted M31 background RR Lyrae density of 0.0077 stars/sq arcsec as derived from the outermost RR Lyrae point based on the observations in the present study. We note that the average density of the seven outermost points from the S09 study ( $R_{\text{major axis}} \geq 300''$ ) is  $0.0068 \pm 0.00070$  stars/sq arcsec, which is consistent with our adopted value.

Adopting the outermost radial point as representative of the M31 background, we subtract this from the RC and RR Lyrae distributions and plot the result in the lower panel of Fig. 9 along with the M32 major axis surface brightness profile from Choi et al. (2002). The latter has been scaled to fit the RC profile outside of 90 arcsec. We see that the RC and RR Lyrae star radial distributions agree from  $\approx 100''$  out to the limit of the data. These in turn are consistent with the shape of the surface brightness profile from Choi et al. (2002). In contrast, the innermost RR Lyrae point at  $\approx 77''$  is significantly below the RC profile at that location. This is

**Table 2.** ab-type RR Lyraes in M32 WFC1 Field

Star ID	R. A. (J2000)	Dec (J2000)	$\langle V \rangle$	$\langle I \rangle$	$(V-I)_{min}$	$\langle V-I \rangle$	Period (days)	V Amplitude	I Amplitude
69090	0 42 54.89	+40 49 36.18	25.666	25.001	0.831	0.684	0.5632	0.7199	0.4600
55439	0 42 55.13	+40 50 50.89	25.271	24.610	0.778	0.673	0.6231	0.5623	0.3681
61847	0 42 55.29	+40 51 45.40	25.399	24.790	0.637	0.610	0.5599	0.4055	0.3626
50225	0 42 55.30	+40 50 45.96	25.217	24.628	0.788	0.622	0.5827	0.8878	0.5310
54773	0 42 55.33	+40 50 39.33	25.118	24.606	0.701	0.546	0.5175	0.9801	0.6470
48015	0 42 55.35	+40 50 18.52	25.086	24.581	0.711	0.555	0.5197	1.0407	0.6680
67388	0 42 55.41	+40 50 5.04	25.341	24.893	0.745	0.521	0.4624	1.4403	0.9278
35269	0 42 55.42	+40 50 24.92	25.182	24.525	0.766	0.667	0.8008	0.5904	0.4490
32856	0 42 55.44	+40 51 19.85	25.015	24.474	0.597	0.544	0.6366	0.4060	0.3230
62696	0 42 55.60	+40 50 48.39	25.390	24.781	0.763	0.632	0.4990	0.8992	0.6681
58192	0 42 55.63	+40 49 20.29	25.348	24.681	0.765	0.681	0.5804	0.8005	0.6434
60642	0 42 55.64	+40 51 26.90	25.281	24.740	0.694	0.564	0.5186	0.8485	0.5899
36931	0 42 55.69	+40 52 16.51	25.052	24.484	0.665	0.576	0.6181	0.4570	0.3017
39138	0 42 55.69	+40 51 49.84	25.004	24.477	0.738	0.558	0.6342	0.9047	0.5900
67607	0 42 55.72	+40 51 26.97	25.436	24.834	0.798	0.633	0.5405	0.9463	0.6393
57075	0 42 55.77	+40 51 56.22	25.227	24.674	0.729	0.581	0.5494	0.9114	0.6162
46974	0 42 55.85	+40 52 15.39	24.988	24.486	0.642	0.522	0.5735	0.8828	0.6620
61434	0 42 55.91	+40 51 55.85	25.358	24.869	0.665	0.519	0.5184	0.8336	0.5472
67418	0 42 55.99	+40 52 20.62	25.576	24.985	0.759	0.607	0.5578	0.5900	0.3453
56137	0 42 55.99	+40 50 51.41	25.104	24.644	0.794	0.531	0.5625	1.2596	0.6549
54713	0 42 56.04	+40 51 35.38	25.299	24.656	0.819	0.670	0.6592	0.9284	0.6640
66175	0 42 56.15	+40 52 0.90	25.295	24.866	0.647	0.473	0.4528	1.1573	0.7765
46197	0 42 56.17	+40 50 30.26	25.217	24.577	0.785	0.659	0.6636	0.7309	0.5106
59774	0 42 56.22	+40 52 5.18	25.280	24.790	0.679	0.520	0.4629	0.9408	0.6355
65422	0 42 56.27	+40 50 28.89	25.342	24.862	0.698	0.527	0.5081	1.0731	0.6947
53771	0 42 56.29	+40 51 21.75	25.105	24.562	0.687	0.562	0.6009	0.8018	0.5666
63722	0 42 56.30	+40 50 29.18	25.330	24.791	0.709	0.565	0.5477	0.8941	0.6199
57597	0 42 56.32	+40 49 23.86	25.214	24.686	0.720	0.563	0.4698	0.9847	0.6450
64241	0 42 56.34	+40 49 30.91	25.309	24.812	0.670	0.522	0.5669	0.6889	0.3641
63704	0 42 56.36	+40 50 12.23	25.445	24.848	0.721	0.613	0.6250	0.6865	0.4734
65777	0 42 56.41	+40 49 50.05	25.399	24.735	0.785	0.683	0.5753	0.8467	0.6445
59544	0 42 56.44	+40 50 51.66	25.358	24.765	0.733	0.605	0.6034	0.5138	0.3065
51592	0 42 56.51	+40 51 51.01	25.105	24.550	0.725	0.580	0.6307	0.9315	0.6757
61625	0 42 56.57	+40 52 15.86	25.399	24.870	0.673	0.543	0.4991	0.6685	0.4861
48996	0 42 56.57	+40 52 2.45	25.199	24.586	0.755	0.628	0.6675	0.6328	0.4273
45777	0 42 56.61	+40 52 15.39	25.227	24.666	0.788	0.588	0.5462	0.7699	0.4139
60305	0 42 56.62	+40 50 13.15	25.261	24.736	0.725	0.572	0.5157	1.0637	0.7044
64071	0 42 56.62	+40 50 10.03	25.310	24.812	0.757	0.553	0.4863	1.1786	0.7131
73214	0 42 56.67	+40 52 21.06	25.520	25.076	0.689	0.484	0.4538	1.0570	0.6715
58708	0 42 56.68	+40 49 28.03	25.221	24.729	0.690	0.521	0.5306	0.9565	0.6548
49905	0 42 56.84	+40 50 52.61	25.135	24.532	0.830	0.640	0.6290	0.9961	0.6409
56022	0 42 57.03	+40 50 0.12	25.280	24.657	0.696	0.626	0.6122	0.3570	0.2582
30515	0 42 57.10	+40 49 34.48	25.028	24.362	0.670	0.667	0.8009	0.2962	0.2904
59434	0 42 57.11	+40 51 14.59	25.245	24.757	0.564	0.500	0.4622	0.6359	0.4945
48065	0 42 57.25	+40 49 33.99	25.078	24.505	0.633	0.580	0.6801	0.4055	0.2953
58892	0 42 57.29	+40 50 49.83	25.316	24.660	0.825	0.679	0.5175	0.7926	0.5379
59021	0 42 57.40	+40 52 4.61	25.223	24.684	0.656	0.553	0.5869	0.6420	0.4690
60828	0 42 57.48	+40 52 8.76	25.215	24.785	0.653	0.470	0.4783	0.8746	0.4788
48098	0 42 57.50	+40 50 41.62	25.209	24.531	0.897	0.710	0.4991	0.9126	0.5784
53889	0 42 57.54	+40 49 14.81	25.105	24.652	0.656	0.484	0.5601	1.0170	0.7095
63400	0 42 57.67	+40 50 49.04	25.333	24.814	0.699	0.547	0.5037	0.9899	0.7216
61232	0 42 57.72	+40 50 18.18	25.387	24.775	0.720	0.623	0.6088	0.6151	0.4465
66556	0 42 57.74	+40 51 14.26	25.358	24.901	0.612	0.488	0.4747	0.8969	0.6317
58733	0 42 57.80	+40 49 14.75	25.231	24.661	0.735	0.598	0.5756	0.7333	0.4279
57789	0 42 57.89	+40 50 48.88	25.183	24.628	0.716	0.580	0.6277	0.9722	0.7329
65004	0 42 57.90	+40 51 25.07	25.516	24.868	0.792	0.665	0.5344	0.7206	0.4965
58702	0 42 57.91	+40 51 3.32	25.274	24.688	0.784	0.610	0.5710	0.7200	0.4180
59373	0 42 57.93	+40 50 3.77	25.287	24.747	0.799	0.584	0.5623	0.9798	0.5123
57450	0 42 57.94	+40 50 56.93	25.303	24.655	0.713	0.654	0.5928	0.4984	0.3806
61406	0 42 57.95	+40 50 26.58	25.411	24.778	0.783	0.649	0.5762	0.6861	0.4505
57217	0 42 58.05	+40 50 26.24	25.328	24.643	0.916	0.734	0.5009	1.1612	0.7672
60341	0 42 58.12	+40 51 7.31	25.533	24.955	0.710	0.606	0.9759	0.9464	0.7199
31984	0 42 58.20	+40 51 3.21	25.033	24.411	0.798	0.651	0.5915	0.7720	0.4505
60733	0 42 58.25	+40 49 36.88	25.256	24.759	0.614	0.517	0.4890	0.9042	0.6977
30172	0 42 58.29	+40 49 14.21	25.064	24.429	0.787	0.655	0.6001	0.8050	0.5731
58034	0 42 58.35	+40 51 24.01	25.194	24.698	0.724	0.531	0.5675	0.5148	0.3200
57984	0 42 58.35	+40 51 25.06	25.232	24.740	0.619	0.504	0.5581	0.6657	0.2222

**Table 3.** c-type RR Lyraes in M32 WFC1 Field

Star ID	R. A. (J2000)	Dec (J2000)	$\langle V \rangle$	$\langle I \rangle$	$(V-I)_{min}$	$\langle V-I \rangle$	Period (days)	V Amplitude	I Amplitude
55904	0 42 55.28	+40 50 41.80	25.223	24.707	0.625	0.525	0.3358	0.3853	0.2382
62969	0 42 55.37	+40 52 28.13	25.351	24.976	0.478	0.384	0.3177	0.4386	0.2929
57604	0 42 55.69	+40 49 58.02	25.223	24.741	0.620	0.492	0.3629	0.4065	0.2225
47179	0 42 55.79	+40 49 32.05	25.108	24.696	0.490	0.417	0.3836	0.3765	0.2668
62947	0 42 55.94	+40 51 42.68	25.323	24.958	0.467	0.373	0.3050	0.4364	0.2886
62331	0 42 56.01	+40 51 36.24	25.292	24.984	0.407	0.317	0.2760	0.4680	0.3216
46671	0 42 56.12	+40 51 9.32	25.090	24.667	0.519	0.431	0.3759	0.3684	0.2302
64272	0 42 56.28	+40 50 50.67	25.443	24.998	0.621	0.458	0.3132	0.4383	0.2006
65746	0 42 56.41	+40 49 33.70	25.471	24.946	0.627	0.535	0.4447	0.4610	0.3253
59461	0 42 56.69	+40 51 56.99	25.256	24.837	0.505	0.425	0.3172	0.3701	0.2512
58682	0 42 56.74	+40 52 17.35	25.210	24.765	0.496	0.448	0.3203	0.2996	0.2272
61581	0 42 56.82	+40 52 32.35	25.274	24.938	0.319	0.336	0.2672	0.2027	0.2314
53785	0 42 57.28	+40 51 13.01	25.147	24.737	0.559	0.424	0.3375	0.5130	0.3116
56798	0 42 57.66	+40 52 30.52	25.229	24.880	0.414	0.355	0.3159	0.4741	0.3693
73248	0 42 57.74	+40 50 6.20	25.627	25.192	0.460	0.437	0.2595	0.3338	0.3024
51794	0 42 57.91	+40 52 2.09	25.118	24.691	0.459	0.430	0.3468	0.2636	0.2224
48903	0 42 57.96	+40 50 10.13	25.180	24.657	0.533	0.524	0.3003	0.3360	0.3225
55347	0 42 58.10	+40 50 28.07	25.188	24.673	0.616	0.521	0.4049	0.3520	0.2186
63681	0 42 58.11	+40 49 23.12	25.318	24.997	0.455	0.333	0.2794	0.4605	0.2563
60749	0 42 58.19	+40 50 38.24	25.346	24.832	0.682	0.528	0.3435	0.4361	0.2044
46986	0 42 59.16	+40 49 34.93	25.086	24.628	0.607	0.470	0.3791	0.4355	0.2248
65451	0 42 59.40	+40 49 41.65	25.381	25.042	0.404	0.343	0.2362	0.3023	0.2000
63777	0 42 59.48	+40 51 25.40	25.314	24.936	0.473	0.386	0.2897	0.4306	0.2889
55590	0 42 59.62	+40 49 44.82	25.083	24.693	0.444	0.395	0.2815	0.3897	0.3072
58269	0 42 59.78	+40 51 50.22	25.266	24.824	0.555	0.451	0.3005	0.4017	0.2496
65019	0 42 59.78	+40 51 53.26	25.357	24.985	0.472	0.381	0.2725	0.4725	0.3248
62830	0 42 59.90	+40 52 19.36	25.331	24.925	0.544	0.417	0.2805	0.4582	0.2687
57577	0 43 0.14	+40 49 51.76	25.203	24.797	0.507	0.413	0.3118	0.3936	0.2520
40622	0 43 0.27	+40 52 0.49	25.050	24.561	0.619	0.499	0.3864	0.3806	0.2000
56582	0 43 0.51	+40 52 24.38	25.180	24.737	0.522	0.451	0.3850	0.5565	0.4484
43206	0 43 0.52	+40 52 31.33	25.059	24.695	0.410	0.367	0.3370	0.2795	0.2000
55323	0 43 0.78	+40 52 3.30	25.170	24.797	0.474	0.379	0.2586	0.3484	0.2007
59222	0 43 1.31	+40 49 51.58	25.200	24.730	0.537	0.475	0.3471	0.3600	0.2699
57384	0 43 1.70	+40 52 34.85	25.229	24.874	0.465	0.362	0.3005	0.3744	0.2120
59319	0 43 1.72	+40 52 14.40	25.286	24.830	0.610	0.468	0.3268	0.4346	0.2278
59796	0 43 1.75	+40 49 34.49	25.227	24.823	0.457	0.409	0.3269	0.4050	0.3259
47221	0 43 1.76	+40 51 57.59	25.025	24.613	0.524	0.420	0.3672	0.3828	0.2195
59930	0 43 1.77	+40 51 33.82	25.236	24.793	0.604	0.455	0.3353	0.4400	0.2225
54765	0 43 1.80	+40 51 29.67	25.151	24.688	0.543	0.470	0.3550	0.4079	0.3041
71755	0 43 2.18	+40 50 18.40	25.623	25.096	0.700	0.543	0.4105	0.4716	0.2356
61260	0 43 2.24	+40 51 24.58	25.280	24.815	0.531	0.470	0.3073	0.3721	0.2824
66764	0 43 2.25	+40 49 52.11	25.397	25.000	0.501	0.407	0.2779	0.4857	0.3353
58941	0 43 2.40	+40 51 7.25	25.240	24.786	0.476	0.455	0.2559	0.2564	0.2276
71318	0 43 2.54	+40 49 28.92	25.606	25.115	0.556	0.496	0.3102	0.4102	0.3221
57831	0 43 2.57	+40 50 0.87	25.159	24.737	0.495	0.427	0.3368	0.3658	0.2598
60022	0 43 2.92	+40 51 2.56	25.235	24.825	0.486	0.415	0.3342	0.3882	0.2801
61747	0 43 3.11	+40 50 32.69	25.363	24.851	0.622	0.519	0.3370	0.3444	0.2000
65449	0 43 3.25	+40 50 41.22	25.358	25.015	0.384	0.347	0.2784	0.4376	0.3784
55403	0 43 3.31	+40 50 31.00	25.183	24.658	0.567	0.527	0.3736	0.3080	0.2497
60273	0 43 3.37	+40 49 35.06	25.275	24.800	0.585	0.484	0.3459	0.4156	0.2620
60983	0 43 3.73	+40 51 24.99	25.310	24.831	0.528	0.481	0.3353	0.3085	0.2440
30529	0 43 3.90	+40 52 30.59	24.963	24.531	0.454	0.434	0.4067	0.3388	0.3088

most likely a result of the fact that our detection and characterization of RR Lyraes in the inner regions of M32 has been adversely affected by the high stellar crowding. These are not accounted for in our assessment of photometric completeness and are more pronounced as the center of M32 is approached.

As mentioned above, Fig. 9 shows that the RR Lyraes follow the RC radial profile very closely, which in turn follows the M32 surface brightness profile from Choi et al.

(2002). This suggests that a significant fraction of the RR Lyraes in this ACS field belong to M32. As a result, this is evidence that M32 contains RR Lyrae variables and therefore a population older than  $\approx 10$  Gyr.

In order to estimate the number of RR Lyraes that likely belong to M32 in this field, we integrate the RR Lyrae radial profile in the lower panel of Fig. 9, which is the one that is background-subtracted and completeness corrected. Doing this, we find 222 RR Lyraes in this field that belong

**Table 4.** ab-type RR Lyraes in M32 WFC2 Field

Star ID	R. A. (J2000)	Dec (J2000)	$\langle V \rangle$	$\langle I \rangle$	$(V-I)_{min}$	$\langle V-I \rangle$	Period (days)	V Amplitude	I Amplitude
161985	0 42 45.81	+40 50 29.49	25.407	24.774	0.768	0.648	0.5709	0.6127	0.4081
124879	0 42 45.86	+40 49 15.40	25.238	24.708	0.620	0.540	0.5760	0.6285	0.4898
119671	0 42 46.02	+40 50 55.64	25.299	24.872	0.507	0.437	0.5869	0.9324	0.8322
145978	0 42 46.03	+40 50 40.41	25.160	24.752	0.592	0.445	0.4481	1.0279	0.7026
131710	0 42 46.04	+40 50 38.09	25.260	24.904	0.375	0.358	0.7845	0.4529	0.4138
160482	0 42 46.11	+40 50 32.97	25.471	24.800	0.834	0.696	0.5253	0.8770	0.6202
170827	0 42 46.14	+40 50 23.19	25.412	24.920	0.673	0.523	0.4562	0.9407	0.6043
113542	0 42 46.15	+40 50 24.89	25.180	24.513	0.690	0.668	0.7671	0.2416	0.2109
117691	0 42 46.15	+40 50 58.37	25.024	24.603	0.540	0.434	0.5676	0.6623	0.4599
135795	0 42 46.17	+40 52 12.82	25.282	24.736	0.655	0.559	0.5682	0.6109	0.4066
164591	0 42 46.18	+40 49 29.34	25.464	24.919	0.688	0.569	0.5382	0.7451	0.4868
158511	0 42 46.19	+40 49 13.29	25.421	24.785	0.661	0.637	0.6374	0.3680	0.3300
108241	0 42 46.35	+40 49 15.78	25.146	24.559	0.707	0.599	0.6470	0.5707	0.3874
160121	0 42 46.37	+40 49 28.57	25.465	24.826	0.771	0.654	0.5878	0.6338	0.4343
92629	0 42 46.38	+40 49 26.58	25.040	24.497	0.760	0.573	0.7857	0.8131	0.4387
107737	0 42 46.39	+40 51 30.61	25.231	24.571	0.810	0.675	0.6793	0.5897	0.3393
154426	0 42 46.43	+40 49 34.41	25.461	24.898	0.764	0.592	0.5493	0.9146	0.6102
113345	0 42 46.43	+40 50 19.96	25.167	24.646	0.637	0.539	0.5913	0.8892	0.7094
152106	0 42 46.49	+40 51 16.67	25.273	24.736	0.675	0.558	0.5470	0.8647	0.6437
182941	0 42 46.49	+40 51 46.80	25.591	25.249	0.372	0.347	0.5788	0.7732	0.7192
165040	0 42 46.49	+40 50 58.95	25.444	24.987	0.677	0.482	0.5600	0.7678	0.4180
107394	0 42 46.53	+40 50 46.62	25.113	24.516	0.657	0.601	0.7216	0.4600	0.3814
154337	0 42 46.55	+40 49 10.28	25.297	24.805	0.550	0.497	0.4745	0.4042	0.3040
169583	0 42 46.57	+40 50 51.92	25.560	24.959	0.682	0.612	0.4490	0.7394	0.6205
91142	0 42 46.58	+40 51 49.91	25.043	24.510	0.719	0.562	0.4984	0.8283	0.4855
68329	0 42 46.63	+40 51 59.88	24.865	24.136	0.823	0.740	0.5117	0.6161	0.4471
172607	0 42 46.63	+40 51 0.96	25.625	25.010	0.799	0.634	0.6194	0.6472	0.3560
114308	0 42 46.64	+40 50 1.81	25.130	24.558	0.730	0.594	0.5353	0.8815	0.6433
140934	0 42 46.67	+40 51 30.23	25.209	24.675	0.586	0.541	0.5328	0.7162	0.6327
125160	0 42 46.70	+40 50 24.74	25.150	24.512	0.801	0.650	0.8516	0.4989	0.2848
93185	0 42 46.70	+40 49 30.72	25.034	24.503	0.626	0.542	0.5855	0.6420	0.4846
169960	0 42 46.74	+40 52 4.14	25.528	24.967	0.733	0.584	0.5405	0.7773	0.5183
140155	0 42 46.75	+40 49 38.67	25.178	24.632	0.700	0.572	0.5816	0.9932	0.7565
129251	0 42 46.78	+40 50 57.56	25.265	24.611	0.713	0.661	0.6625	0.5906	0.4902
132853	0 42 46.84	+40 50 3.15	25.084	24.687	0.675	0.452	0.4574	1.1859	0.6940
87068	0 42 46.85	+40 50 16.42	25.083	24.561	0.684	0.544	0.5686	0.8046	0.5075
113219	0 42 46.87	+40 50 6.04	25.255	24.626	0.875	0.672	0.5340	0.9800	0.5419
70178	0 42 46.91	+40 51 14.00	25.001	24.240	0.997	0.789	0.8437	0.7161	0.3659
173547	0 42 46.95	+40 50 8.65	25.500	25.011	0.667	0.513	0.4838	0.8451	0.5597
90109	0 42 47.01	+40 50 52.47	24.922	24.402	0.730	0.559	0.5469	1.0868	0.7458
107856	0 42 47.05	+40 49 40.10	25.105	24.567	0.611	0.549	0.6303	0.6242	0.4893
121538	0 42 47.05	+40 52 20.68	25.126	24.508	0.752	0.639	0.5222	0.9212	0.7264
165305	0 42 47.07	+40 51 29.27	25.435	24.883	0.716	0.582	0.5040	1.0062	0.7357
116548	0 42 47.07	+40 50 35.76	25.403	24.704	0.871	0.720	0.6109	0.7005	0.4185
160146	0 42 47.15	+40 50 42.61	25.411	24.831	0.672	0.594	0.5164	0.7963	0.6431
89997	0 42 47.15	+40 51 56.71	25.075	24.535	0.667	0.555	0.5407	0.6740	0.4514
165557	0 42 47.22	+40 51 38.23	25.392	24.808	0.730	0.600	0.4894	0.9344	0.5886
165556	0 42 47.23	+40 49 38.41	25.378	24.827	0.755	0.585	0.5979	0.8539	0.4664
143753	0 42 47.25	+40 51 48.65	25.420	24.671	0.906	0.770	0.5515	0.5812	0.2912
141847	0 42 47.26	+40 49 29.71	25.330	24.743	0.704	0.599	0.5952	0.5552	0.3737
177505	0 42 47.32	+40 49 34.40	25.660	25.084	0.816	0.618	0.5335	1.0226	0.6204
173043	0 42 47.35	+40 51 35.99	25.673	24.983	0.919	0.733	0.5478	1.0121	0.5900
148488	0 42 47.40	+40 50 1.01	25.286	24.689	0.665	0.603	0.6175	0.4271	0.3196
161225	0 42 47.41	+40 50 41.43	25.388	25.057	0.404	0.339	0.4773	0.7005	0.5873
154526	0 42 47.49	+40 51 27.43	25.351	24.758	0.650	0.598	0.5660	0.5716	0.4819
149128	0 42 47.57	+40 51 40.34	25.248	24.784	0.690	0.504	0.5155	1.0485	0.6685
148667	0 42 47.58	+40 49 43.69	25.229	24.620	0.750	0.631	0.5286	0.8331	0.6047
88938	0 42 47.59	+40 52 23.31	25.095	24.470	0.639	0.626	0.5486	0.5906	0.5641
154639	0 42 47.61	+40 52 5.14	25.318	24.801	0.654	0.534	0.5280	0.7381	0.5158
170840	0 42 47.61	+40 50 29.91	25.477	24.995	0.579	0.502	0.5219	0.8500	0.6702
149426	0 42 47.61	+40 50 16.01	25.318	24.761	0.636	0.567	0.6385	0.4981	0.3559
155481	0 42 47.68	+40 51 0.71	25.211	24.779	0.573	0.453	0.4648	0.8760	0.6305
146570	0 42 47.69	+40 51 8.69	25.228	24.652	0.765	0.606	0.5113	0.7190	0.3816
141115	0 42 47.73	+40 52 25.81	25.288	24.738	0.724	0.579	0.5670	0.9830	0.7146
154585	0 42 47.79	+40 51 16.82	25.274	24.770	0.626	0.526	0.4820	0.8449	0.6290
139135	0 42 47.80	+40 50 0.67	25.319	24.749	0.625	0.573	0.5910	0.3711	0.2992
168890	0 42 47.87	+40 51 20.96	25.437	24.884	0.554	0.553	0.6557	0.5540	0.5531

**Table 5.** c-type RR Lyraes in M32 WFC2 Field

Star ID	R. A. (J2000)	Dec (J2000)	$\langle V \rangle$	$\langle I \rangle$	$(V-I)_{min}$	$\langle V-I \rangle$	Period (days)	V Amplitude	I Amplitude
163374	0 42 45.64	+40 49 42.33	25.324	24.961	0.403	0.366	0.3409	0.3612	0.2910
140009	0 42 45.76	+40 49 35.26	25.256	24.761	0.592	0.502	0.3209	0.3690	0.2131
81800	0 42 46.41	+40 52 8.19	25.053	24.267	0.846	0.793	0.3529	0.5520	0.4156
121539	0 42 46.52	+40 49 12.69	25.193	24.692	0.524	0.502	0.3424	0.3508	0.3187
123696	0 42 46.54	+40 50 55.11	25.218	24.673	0.587	0.548	0.2986	0.3276	0.2707
178394	0 42 46.57	+40 50 29.67	25.539	25.159	0.433	0.385	0.2841	0.4103	0.3262
157733	0 42 46.63	+40 50 22.54	25.236	24.847	0.439	0.393	0.3090	0.4810	0.3972
140928	0 42 46.80	+40 50 4.68	25.253	24.748	0.578	0.510	0.2951	0.3299	0.2305
135720	0 42 48.14	+40 52 27.47	25.209	24.824	0.496	0.394	0.3686	0.4117	0.2483
171457	0 42 48.30	+40 50 12.36	25.377	24.957	0.549	0.430	0.3105	0.3859	0.2000
178596	0 42 48.50	+40 50 31.61	25.503	25.111	0.438	0.396	0.2510	0.3541	0.2824
110363	0 42 48.53	+40 51 43.71	25.084	24.615	0.551	0.475	0.3583	0.3592	0.2518
149671	0 42 48.60	+40 52 24.18	25.292	24.968	0.454	0.334	0.2941	0.3991	0.2000
185213	0 42 48.64	+40 50 58.36	25.736	25.190	0.546	0.546	0.3202	0.3832	0.3827
132509	0 42 48.75	+40 51 21.97	25.180	24.760	0.475	0.424	0.4388	0.3065	0.2293
176174	0 42 48.77	+40 51 26.81	25.513	25.142	0.384	0.372	0.2479	0.3654	0.3466
144964	0 42 49.03	+40 50 2.41	25.182	24.833	0.447	0.356	0.2872	0.4056	0.2590
127615	0 42 49.27	+40 50 22.59	25.150	24.689	0.552	0.467	0.2949	0.3657	0.2370
168074	0 42 49.29	+40 51 51.25	25.447	25.103	0.402	0.348	0.2946	0.3866	0.3000
158000	0 42 49.32	+40 51 44.83	25.346	24.888	0.560	0.465	0.2856	0.3940	0.2577
97401	0 42 49.36	+40 49 58.65	25.127	24.480	0.753	0.655	0.3671	0.3626	0.2144
134366	0 42 49.42	+40 52 16.10	25.122	24.658	0.557	0.470	0.3920	0.3349	0.2033
87529	0 42 49.49	+40 51 18.52	25.055	24.544	0.571	0.515	0.3273	0.3420	0.2650
130739	0 42 49.73	+40 50 25.33	25.158	24.741	0.506	0.422	0.3130	0.3254	0.2000
152681	0 42 49.82	+40 49 34.93	25.179	24.826	0.372	0.354	0.2853	0.3639	0.3300
118971	0 42 49.87	+40 51 50.22	25.226	24.680	0.662	0.555	0.2635	0.4039	0.2457
142906	0 42 49.89	+40 50 6.57	25.196	24.828	0.428	0.373	0.3320	0.4141	0.3188
115358	0 42 50.21	+40 50 14.29	25.062	24.636	0.477	0.429	0.3237	0.2720	0.2000
107079	0 42 50.33	+40 51 37.81	25.100	24.736	0.440	0.370	0.3237	0.3560	0.2365
172768	0 42 50.35	+40 49 21.63	25.456	25.088	0.451	0.374	0.2661	0.3868	0.2648
179524	0 42 50.48	+40 49 54.87	25.614	25.107	0.570	0.511	0.2281	0.2821	0.2000
146744	0 42 50.57	+40 49 25.77	25.208	24.701	0.549	0.510	0.3727	0.3300	0.2727
118405	0 42 50.57	+40 50 1.12	25.126	24.619	0.595	0.514	0.3100	0.3937	0.2803
166477	0 42 50.62	+40 52 10.73	25.331	25.017	0.386	0.318	0.2814	0.3208	0.2134
155316	0 42 50.72	+40 50 27.53	25.336	24.879	0.506	0.460	0.2790	0.3300	0.2658
122176	0 42 50.76	+40 50 1.40	25.116	24.621	0.586	0.501	0.4181	0.3200	0.2001
139320	0 42 50.83	+40 49 21.06	25.085	24.710	0.436	0.379	0.3549	0.3130	0.2185
130418	0 42 50.84	+40 51 40.29	25.137	24.783	0.405	0.358	0.3253	0.3246	0.2524
165432	0 42 50.88	+40 49 57.58	25.391	24.977	0.487	0.420	0.3254	0.3657	0.2645
158948	0 42 50.90	+40 50 44.02	25.352	24.859	0.643	0.505	0.3696	0.4535	0.2553
163589	0 42 50.93	+40 50 1.01	25.385	24.920	0.512	0.468	0.3421	0.3299	0.2659
98796	0 42 50.93	+40 50 50.00	24.979	24.502	0.557	0.481	0.3955	0.3089	0.2030
161634	0 42 50.99	+40 50 28.97	25.309	24.948	0.469	0.371	0.3116	0.4546	0.2935
188945	0 42 51.03	+40 50 14.54	25.623	25.228	0.465	0.400	0.2702	0.4417	0.3218
158766	0 42 51.23	+40 49 14.97	25.319	24.874	0.564	0.452	0.3122	0.3924	0.2327
167658	0 42 51.39	+40 51 52.37	25.409	24.994	0.568	0.427	0.2660	0.4306	0.2103
175094	0 42 51.56	+40 49 37.65	25.455	25.117	0.406	0.345	0.2717	0.4556	0.3433
110475	0 42 51.61	+40 52 29.00	25.000	24.525	0.553	0.482	0.4100	0.4193	0.3204
159096	0 42 51.66	+40 50 3.28	25.323	24.840	0.541	0.487	0.3637	0.3600	0.2808
105794	0 42 51.88	+40 49 47.46	25.063	24.636	0.544	0.434	0.3806	0.3623	0.2000
115435	0 42 52.00	+40 50 46.30	25.051	24.635	0.448	0.419	0.3277	0.4264	0.3570
167757	0 42 52.01	+40 51 7.01	25.341	24.934	0.493	0.414	0.2779	0.4014	0.2750
156984	0 42 52.12	+40 49 10.20	25.233	24.885	0.347	0.348	0.3482	0.3628	0.3643
148036	0 42 52.14	+40 49 30.85	25.288	24.874	0.575	0.427	0.3083	0.4600	0.2399
136940	0 42 52.32	+40 52 28.32	25.221	24.732	0.606	0.497	0.2781	0.3737	0.2090
156828	0 42 52.43	+40 49 51.37	25.322	24.872	0.517	0.454	0.3243	0.3294	0.2379
123312	0 42 52.43	+40 52 13.30	25.122	24.701	0.467	0.424	0.3829	0.3051	0.2367
158838	0 42 52.44	+40 50 52.25	25.383	24.881	0.617	0.515	0.2783	0.4979	0.3196
178736	0 42 52.51	+40 51 43.57	25.546	25.069	0.607	0.486	0.3081	0.3837	0.2087
128375	0 42 52.55	+40 50 24.18	25.204	24.669	0.612	0.539	0.2768	0.3068	0.2000
194657	0 42 52.57	+40 51 42.69	25.704	25.312	0.508	0.399	0.4264	0.3656	0.2000
178291	0 42 52.66	+40 51 34.09	25.555	25.097	0.659	0.474	0.2577	0.4910	0.2214
170435	0 42 52.71	+40 52 13.38	25.502	25.081	0.539	0.430	0.2894	0.4260	0.2650
95585	0 42 52.86	+40 49 39.56	24.939	24.508	0.562	0.444	0.4057	0.5470	0.3742
124197	0 42 52.93	+40 50 1.22	25.195	24.638	0.650	0.566	0.3738	0.4209	0.2961
144357	0 42 53.08	+40 50 29.27	25.274	24.680	0.659	0.598	0.4044	0.3198	0.2326
100706	0 42 53.12	+40 52 23.94	25.045	24.655	0.363	0.360	0.3513	0.2049	0.2000

**Table 6.** ab-type RR Lyraes in Control WFC1 Field

Star ID	R. A. (J2000)	Dec (J2000)	$\langle V \rangle$	$\langle I \rangle$	$(V-I)_{min}$	$\langle V-I \rangle$	Period (days)	V Amplitude	I Amplitude
59041	0 43 27.88	+41 4 26.80	25.055	24.599	0.555	0.472	0.5134	0.7479	0.5663
80706	0 43 27.89	+41 2 14.93	25.348	24.858	0.579	0.503	0.5276	0.6531	0.5057
75357	0 43 27.93	+41 4 54.96	25.370	24.817	0.632	0.559	0.6035	0.4618	0.3593
74424	0 43 27.95	+41 4 26.71	25.264	24.756	0.648	0.527	0.5516	0.8250	0.6131
63686	0 43 27.95	+41 4 0.55	25.216	24.628	0.809	0.626	0.5834	1.0540	0.7148
90791	0 43 28.00	+41 3 5.46	25.685	24.996	0.682	0.688	0.5469	0.3511	0.3626
68832	0 43 28.16	+41 2 45.91	25.193	24.721	0.614	0.493	0.5600	0.8514	0.6097
63982	0 43 28.20	+41 3 36.75	25.221	24.738	0.758	0.525	0.4881	0.9670	0.5556
64771	0 43 28.41	+41 3 50.75	25.314	24.668	0.699	0.649	0.6245	0.3676	0.2873
63577	0 43 28.42	+41 2 21.45	25.199	24.705	0.642	0.516	0.5981	0.8829	0.6497
58709	0 43 28.44	+41 2 18.15	25.219	24.610	0.720	0.618	0.7544	0.5729	0.4288
64746	0 43 28.45	+41 2 10.27	25.315	24.668	0.697	0.651	0.6772	0.5396	0.4600
75215	0 43 28.53	+41 4 16.32	25.317	24.874	0.508	0.454	0.5000	0.7192	0.5900
58116	0 43 28.56	+41 4 1.85	25.313	24.668	0.764	0.654	0.5979	0.4361	0.2572
41845	0 43 28.59	+41 5 26.09	25.073	24.477	0.745	0.614	0.5822	0.7713	0.5424
49857	0 43 28.61	+41 5 16.08	25.188	24.562	0.731	0.633	0.7429	0.4340	0.2959
29915	0 43 28.61	+41 5 3.28	24.989	24.353	0.831	0.662	0.6600	0.7907	0.4687
74909	0 43 28.69	+41 4 7.51	25.378	24.767	0.710	0.617	0.6580	0.4046	0.2728
30014	0 43 28.70	+41 3 49.67	24.902	24.238	0.742	0.670	0.7934	0.4416	0.3387
77732	0 43 28.80	+41 3 23.00	25.445	24.834	0.745	0.624	0.6077	0.6132	0.4179
81465	0 43 28.83	+41 3 49.78	25.447	24.897	0.648	0.558	0.6074	0.5276	0.4014
83470	0 43 28.86	+41 4 54.47	25.508	24.940	0.748	0.598	0.4888	0.9487	0.6505
79311	0 43 28.87	+41 4 29.38	25.278	24.782	0.601	0.516	0.5104	0.9798	0.7898
43958	0 43 28.94	+41 5 2.69	25.118	24.530	0.667	0.598	0.7818	0.7104	0.5947
79507	0 43 28.97	+41 3 2.66	25.346	24.850	0.633	0.513	0.5500	0.7465	0.5196
71495	0 43 28.99	+41 4 6.52	25.337	24.691	0.844	0.681	0.5083	0.9534	0.6016
42314	0 43 28.99	+41 4 51.71	25.075	24.440	0.848	0.661	0.5531	0.7504	0.4024
79289	0 43 29.08	+41 2 32.19	25.423	24.915	0.636	0.520	0.4860	0.4970	0.2997
76250	0 43 29.11	+41 4 26.86	25.423	24.813	0.694	0.617	0.6100	0.4770	0.3426
72099	0 43 29.12	+41 4 50.44	25.345	24.688	0.715	0.661	0.5977	0.3871	0.3005
77677	0 43 29.18	+41 3 38.98	25.261	24.663	0.753	0.643	0.4868	1.1920	0.9333
81800	0 43 29.29	+41 2 47.38	25.485	24.920	0.682	0.586	0.4598	0.9990	0.8171
39349	0 43 29.35	+41 4 40.27	25.070	24.511	0.665	0.577	0.5368	0.8140	0.6242
78224	0 43 29.41	+41 2 37.49	25.379	24.871	0.698	0.531	0.5386	0.7702	0.4600
66092	0 43 29.41	+41 3 48.82	25.221	24.668	0.682	0.575	0.6395	0.9432	0.7424
79787	0 43 29.45	+41 5 5.69	25.444	24.934	0.655	0.535	0.4512	0.8225	0.5898
28287	0 43 29.54	+41 4 36.72	24.870	24.206	0.827	0.680	0.6912	0.5936	0.3316
75710	0 43 29.54	+41 4 22.53	25.241	24.744	0.684	0.528	0.5965	0.9736	0.6755
66433	0 43 29.59	+41 4 36.62	25.288	24.668	0.645	0.622	0.6575	0.4010	0.3689
81400	0 43 29.63	+41 3 10.15	25.500	24.791	0.897	0.733	0.5502	0.8025	0.5098
80636	0 43 29.66	+41 2 55.01	25.419	24.855	0.654	0.580	0.5240	0.7430	0.5738
65332	0 43 29.69	+41 2 18.72	25.187	24.691	0.681	0.525	0.5840	0.9764	0.6871
81214	0 43 29.72	+41 5 17.13	25.380	24.872	0.598	0.522	0.5160	0.8501	0.7128
47209	0 43 29.75	+41 3 35.19	25.032	24.506	0.651	0.549	0.6168	0.8499	0.6295
93455	0 43 29.76	+41 5 10.24	25.547	25.019	0.688	0.567	0.4443	1.0203	0.7333
83272	0 43 29.77	+41 3 0.74	25.306	24.885	0.648	0.474	0.4982	1.3224	0.9408
73504	0 43 29.78	+41 5 15.95	25.285	24.744	0.606	0.547	0.5833	0.5630	0.4685
33520	0 43 29.79	+41 4 41.21	25.096	24.542	0.785	0.594	0.6020	1.0056	0.6212
77659	0 43 29.80	+41 4 6.78	25.369	24.820	0.750	0.577	0.5543	0.8294	0.5064
82341	0 43 29.99	+41 2 45.07	25.348	24.812	0.655	0.554	0.5239	0.8715	0.6873
75793	0 43 30.00	+41 4 49.76	25.344	24.820	0.684	0.550	0.5110	0.9230	0.6564
58423	0 43 30.02	+41 2 7.98	25.188	24.710	0.542	0.486	0.5287	0.7199	0.6155
38098	0 43 30.03	+41 4 23.88	25.069	24.491	0.681	0.588	0.5780	0.5660	0.4033
75331	0 43 30.06	+41 4 27.24	25.403	24.846	0.654	0.562	0.6552	0.3289	0.2008
44981	0 43 30.07	+41 4 1.29	25.099	24.550	0.701	0.567	0.5586	0.7067	0.4518
88869	0 43 30.10	+41 2 31.08	25.645	25.026	0.713	0.633	0.5143	0.6895	0.5509
70178	0 43 30.11	+41 3 14.02	25.284	24.674	0.799	0.637	0.5565	0.8097	0.4862
91411	0 43 30.13	+41 4 11.35	25.476	24.955	0.623	0.543	0.4719	0.8935	0.7092
89778	0 43 30.16	+41 3 3.79	25.528	24.974	0.816	0.597	0.5087	1.0449	0.6366
45037	0 43 30.22	+41 4 41.30	25.000	24.484	0.657	0.541	0.6279	0.9859	0.7552
73080	0 43 30.24	+41 4 35.89	25.214	24.717	0.726	0.536	0.5648	1.0844	0.7305
62372	0 43 30.37	+41 3 15.35	25.173	24.654	0.779	0.573	0.5788	1.1879	0.7422
29317	0 43 30.48	+41 4 15.05	24.911	24.233	0.700	0.679	0.6444	0.3470	0.3143
63560	0 43 30.53	+41 3 58.93	25.220	24.679	0.653	0.562	0.4500	0.9649	0.7630
46023	0 43 30.54	+41 4 43.76	25.107	24.453	0.782	0.668	0.7127	0.6243	0.4249
76528	0 43 30.65	+41 4 16.23	25.374	24.843	0.698	0.544	0.5887	0.5745	0.3590
56538	0 43 30.67	+41 4 17.89	25.235	24.574	0.939	0.716	0.5859	0.7001	0.7001

**Table 7.** c-type RR Lyraes in Control WFC1 Field

Star ID	R. A. (J2000)	Dec (J2000)	$\langle V \rangle$	$\langle I \rangle$	$(V-I)_{min}$	$\langle V-I \rangle$	Period (days)	V Amplitude	I Amplitude
65042	0 43 27.91	+41 4 41.46	25.173	24.839	0.421	0.340	0.3229	0.3431	0.2088
47031	0 43 27.94	+41 2 9.82	25.031	24.629	0.475	0.407	0.3033	0.3518	0.2256
57030	0 43 28.09	+41 3 25.20	25.223	24.700	0.576	0.528	0.3240	0.4322	0.3611
70608	0 43 28.29	+41 4 3.26	25.249	24.853	0.496	0.404	0.3141	0.4313	0.2836
76098	0 43 28.40	+41 4 0.59	25.440	24.845	0.663	0.600	0.2849	0.3845	0.2912
71804	0 43 28.42	+41 4 20.76	25.190	24.706	0.504	0.485	0.4015	0.2650	0.2377
80532	0 43 28.52	+41 4 46.32	25.366	25.063	0.373	0.310	0.2814	0.4860	0.3638
74229	0 43 28.53	+41 5 7.73	25.280	24.868	0.436	0.414	0.3844	0.3468	0.3087
82794	0 43 28.63	+41 2 55.73	25.406	24.984	0.522	0.431	0.3187	0.4761	0.3411
63825	0 43 28.92	+41 2 28.77	25.049	24.687	0.411	0.366	0.3801	0.3491	0.2663
27432	0 43 29.07	+41 4 38.05	24.851	24.118	0.752	0.734	0.2535	0.2261	0.2000
49599	0 43 29.16	+41 3 47.36	25.057	24.592	0.476	0.465	0.3815	0.2155	0.2000
72632	0 43 29.21	+41 3 51.02	25.263	24.908	0.430	0.360	0.2732	0.3468	0.2266
64365	0 43 29.37	+41 3 7.08	25.249	24.685	0.667	0.573	0.4052	0.4286	0.2951
42868	0 43 29.67	+41 4 48.57	25.038	24.518	0.593	0.524	0.3722	0.3015	0.2003
72878	0 43 29.67	+41 3 19.07	25.301	24.877	0.532	0.433	0.3078	0.4200	0.2650
76460	0 43 29.88	+41 3 20.61	25.340	24.887	0.644	0.474	0.3150	0.5742	0.3137
68256	0 43 30.34	+41 4 3.02	25.218	24.843	0.387	0.376	0.3515	0.3153	0.2983
81940	0 43 30.38	+41 2 22.51	25.362	25.035	0.343	0.329	0.2784	0.3846	0.3597
63289	0 43 30.78	+41 4 14.50	25.159	24.672	0.471	0.486	0.3882	0.2560	0.2766
66473	0 43 30.87	+41 3 23.00	25.205	24.773	0.542	0.440	0.3384	0.4526	0.3040
84828	0 43 30.92	+41 5 0.56	25.389	25.064	0.406	0.331	0.2539	0.3299	0.2003
68986	0 43 31.16	+41 4 14.42	25.285	24.865	0.522	0.429	0.3191	0.4239	0.2783
65521	0 43 31.22	+41 4 11.33	25.234	24.747	0.590	0.494	0.3360	0.3419	0.2050
54613	0 43 31.32	+41 2 35.36	25.111	24.664	0.545	0.454	0.4146	0.3832	0.2506
47555	0 43 31.35	+41 4 59.42	25.034	24.604	0.490	0.434	0.3842	0.3771	0.2953
57192	0 43 31.45	+41 4 36.90	25.100	24.758	0.426	0.350	0.3329	0.4557	0.3236
80738	0 43 31.56	+41 4 15.94	25.347	24.961	0.446	0.391	0.3110	0.4451	0.3574
57418	0 43 31.60	+41 3 56.99	25.098	24.674	0.511	0.432	0.4000	0.4198	0.2959
78389	0 43 31.67	+41 3 44.82	25.331	24.904	0.515	0.434	0.3149	0.4055	0.2863
86179	0 43 31.69	+41 3 21.45	25.517	25.136	0.469	0.389	0.2742	0.4336	0.3023
68412	0 43 31.99	+41 5 23.36	25.261	24.799	0.508	0.464	0.3862	0.3300	0.2690
69052	0 43 32.02	+41 2 47.02	25.182	24.789	0.430	0.396	0.2712	0.3124	0.2434
72788	0 43 32.27	+41 3 9.10	25.252	24.736	0.612	0.523	0.3571	0.3513	0.2206
68632	0 43 32.49	+41 5 21.89	25.197	24.864	0.442	0.341	0.3769	0.3892	0.2269
53085	0 43 32.52	+41 3 10.15	25.090	24.601	0.616	0.500	0.3810	0.4463	0.2712
70566	0 43 32.64	+41 3 57.77	25.189	24.761	0.463	0.430	0.3340	0.3580	0.3065
81784	0 43 32.65	+41 4 41.09	25.385	25.001	0.478	0.391	0.2727	0.4178	0.2779
37747	0 43 32.73	+41 3 1.95	24.997	24.467	0.622	0.537	0.4434	0.3516	0.2263
68946	0 43 32.73	+41 4 46.52	25.250	24.822	0.525	0.434	0.3559	0.4010	0.2680
79969	0 43 32.83	+41 3 52.79	25.457	24.972	0.615	0.496	0.3807	0.4379	0.2580
61963	0 43 32.83	+41 2 43.28	25.114	24.705	0.476	0.414	0.3480	0.3870	0.2878
35985	0 43 32.86	+41 4 33.48	24.924	24.547	0.439	0.380	0.3176	0.3001	0.2000
79083	0 43 32.88	+41 3 5.55	25.437	24.875	0.636	0.567	0.3519	0.3667	0.2691
59678	0 43 32.89	+41 5 25.09	25.287	24.891	0.442	0.399	0.2774	0.3659	0.2936
81866	0 43 32.96	+41 2 32.83	25.301	24.907	0.506	0.402	0.3250	0.4109	0.2533
79804	0 43 33.10	+41 3 1.44	25.250	24.863	0.471	0.394	0.3108	0.4061	0.2801
58026	0 43 33.17	+41 2 54.74	25.132	24.654	0.563	0.484	0.4077	0.3607	0.2499
75304	0 43 33.22	+41 2 57.21	25.318	24.929	0.488	0.395	0.3196	0.3558	0.2062
57420	0 43 33.27	+41 4 34.91	25.210	24.686	0.539	0.526	0.3745	0.3300	0.3103
75059	0 43 33.55	+41 5 19.80	25.288	24.862	0.519	0.434	0.3287	0.4365	0.3114
64129	0 43 33.70	+41 4 8.57	25.236	24.789	0.563	0.455	0.3000	0.3913	0.2261
64427	0 43 33.72	+41 5 23.70	25.194	24.801	0.394	0.393	0.3222	0.2690	0.2676
84642	0 43 34.17	+41 2 48.54	25.357	25.006	0.383	0.353	0.3151	0.3584	0.3117
77430	0 43 34.23	+41 2 17.19	25.327	24.878	0.533	0.455	0.3330	0.3619	0.2492
77263	0 43 34.27	+41 5 17.93	25.314	24.968	0.435	0.354	0.2977	0.4243	0.2859
84874	0 43 34.36	+41 4 51.10	25.412	25.090	0.401	0.329	0.2707	0.4082	0.2892
70522	0 43 34.63	+41 2 44.47	25.216	24.752	0.523	0.467	0.3966	0.3041	0.2259
80828	0 43 34.83	+41 3 53.18	25.344	24.904	0.548	0.448	0.2793	0.4108	0.2635
86436	0 43 35.04	+41 4 35.78	25.458	25.059	0.481	0.404	0.2900	0.3462	0.2278
65285	0 43 35.16	+41 4 39.59	25.258	24.775	0.504	0.485	0.2940	0.3889	0.3614
78591	0 43 35.29	+41 4 17.45	25.326	24.923	0.545	0.414	0.3097	0.4353	0.2310
78079	0 43 35.47	+41 3 1.82	25.308	24.851	0.604	0.469	0.3290	0.4458	0.2390
77767	0 43 35.89	+41 5 13.96	25.331	24.974	0.401	0.359	0.2710	0.3216	0.2572
77067	0 43 35.95	+41 3 59.89	25.290	24.981	0.380	0.315	0.2952	0.3966	0.2715
82043	0 43 35.97	+41 2 45.36	25.349	25.016	0.462	0.344	0.3031	0.4652	0.2699
70715	0 43 36.14	+41 4 51.36	25.345	24.809	0.648	0.545	0.3805	0.3989	0.2532

**Table 8.** ab-type RR Lyraes in Control WFC2 Field

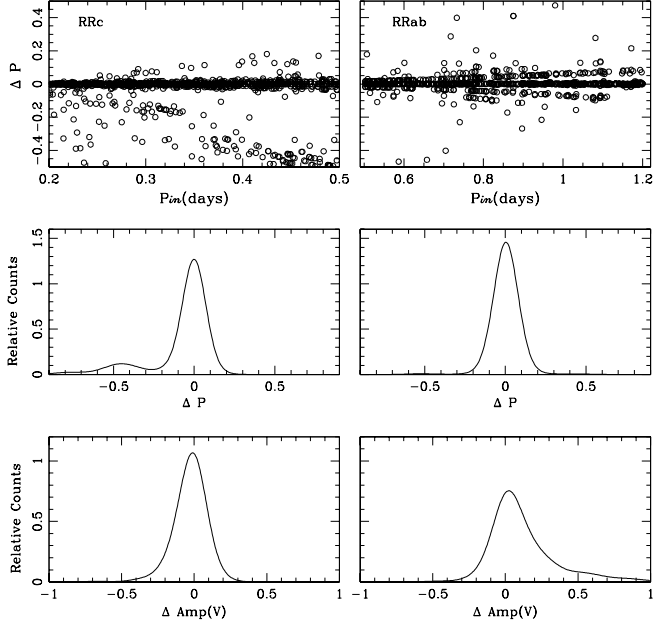
Star ID	R. A. (J2000)	Dec (J2000)	$\langle V \rangle$	$\langle I \rangle$	$(V-I)_{min}$	$\langle V-I \rangle$	Period (days)	V Amplitude	I Amplitude
83936	0 43 18.42	+41 5 8.04	25.314	24.737	0.773	0.602	0.5473	0.7587	0.4600
82752	0 43 18.43	+41 5 14.88	25.255	24.672	0.866	0.630	0.5550	1.0333	0.5900
99546	0 43 18.43	+41 4 33.19	25.372	24.855	0.671	0.536	0.4587	0.6070	0.3421
89174	0 43 18.51	+41 4 24.55	25.305	24.752	0.581	0.557	0.5740	0.5056	0.4549
60763	0 43 18.53	+41 4 47.27	25.208	24.532	0.725	0.679	0.6127	0.4068	0.3328
102771	0 43 18.64	+41 2 60.00	25.269	24.842	0.620	0.472	0.4868	1.2036	0.8786
118814	0 43 18.68	+41 2 6.56	25.490	25.161	0.406	0.342	0.4551	0.7728	0.6389
101753	0 43 18.68	+41 3 34.91	25.198	24.840	0.554	0.403	0.4782	1.1023	0.7328
98770	0 43 18.75	+41 3 55.34	25.310	24.872	0.597	0.462	0.5878	0.9739	0.7317
95761	0 43 18.75	+41 3 39.53	25.321	24.916	0.549	0.430	0.5517	1.0379	0.8052
110846	0 43 18.82	+41 2 20.17	25.477	24.979	0.568	0.509	0.4718	0.8179	0.7199
82597	0 43 18.83	+41 5 13.99	25.251	24.640	0.685	0.619	0.6767	0.6121	0.5064
52935	0 43 18.86	+41 4 59.09	25.127	24.413	0.837	0.724	0.5835	0.5094	0.3082
93064	0 43 18.87	+41 2 2.20	25.223	24.776	0.635	0.487	0.4613	0.9784	0.6252
58545	0 43 18.91	+41 4 6.70	25.129	24.594	0.653	0.546	0.5541	0.5972	0.4093
78156	0 43 18.94	+41 2 6.66	25.168	24.615	0.759	0.587	0.5639	1.0113	0.6916
112921	0 43 18.96	+41 4 33.93	25.451	24.939	0.735	0.542	0.5332	0.8747	0.5297
96585	0 43 18.96	+41 3 23.27	25.288	24.786	0.631	0.515	0.5700	0.6090	0.4131
117275	0 43 19.00	+41 4 45.49	25.463	25.027	0.766	0.514	0.4488	1.2734	0.7132
96650	0 43 19.03	+41 2 24.14	25.347	24.801	0.703	0.564	0.6485	0.6906	0.4652
89462	0 43 19.06	+41 3 34.01	25.235	24.786	0.583	0.475	0.4868	1.0528	0.8079
68308	0 43 19.08	+41 2 54.71	25.159	24.594	0.660	0.575	0.6839	0.5967	0.4599
100640	0 43 19.08	+41 5 6.60	25.396	24.910	0.570	0.494	0.5032	0.5900	0.4600
82951	0 43 19.09	+41 3 22.34	25.197	24.630	0.702	0.587	0.5659	0.8080	0.5892
105288	0 43 19.11	+41 3 18.28	25.456	25.004	0.540	0.465	0.4470	0.9818	0.8491
79252	0 43 19.14	+41 3 40.83	25.167	24.601	0.690	0.587	0.5200	0.9410	0.7449
49770	0 43 19.17	+41 3 11.09	25.124	24.495	0.757	0.649	0.4439	0.6676	0.4348
102821	0 43 19.19	+41 1 56.70	25.481	24.938	0.696	0.560	0.5962	0.6499	0.4294
93016	0 43 19.24	+41 2 55.56	25.339	24.843	0.652	0.520	0.5012	0.9384	0.6943
58893	0 43 19.25	+41 2 17.80	25.114	24.522	0.646	0.596	0.7663	0.4854	0.4028
53855	0 43 19.25	+41 5 12.46	25.106	24.478	0.803	0.645	0.5267	0.5785	0.3222
94030	0 43 19.28	+41 3 10.31	25.390	24.767	0.711	0.630	0.6185	0.3697	0.2290
90683	0 43 19.29	+41 4 27.82	25.248	24.735	0.707	0.545	0.5165	0.9666	0.6430
104544	0 43 19.35	+41 2 47.46	25.430	24.895	0.656	0.549	0.5833	0.6835	0.5120
72779	0 43 19.39	+41 3 7.85	25.239	24.647	0.708	0.601	0.7340	0.4579	0.2860
99716	0 43 19.39	+41 2 27.46	25.326	24.823	0.604	0.517	0.4983	0.6338	0.4844
78117	0 43 19.40	+41 4 51.22	25.287	24.715	0.761	0.593	0.5445	0.7127	0.4162
89225	0 43 19.41	+41 4 48.09	25.334	24.801	0.651	0.544	0.5952	0.5655	0.3780
56712	0 43 19.43	+41 5 10.83	25.149	24.529	0.760	0.635	0.6110	0.6057	0.3681
98171	0 43 19.51	+41 3 44.02	25.376	25.027	0.557	0.396	0.4424	1.0967	0.7047
95996	0 43 19.57	+41 5 10.25	25.456	24.726	0.755	0.731	0.6273	0.3034	0.2697
98161	0 43 19.58	+41 3 29.08	25.273	24.800	0.590	0.491	0.4949	0.9084	0.7359
88292	0 43 19.68	+41 2 3.71	25.084	24.579	0.716	0.536	0.6626	0.9727	0.6542
99375	0 43 19.72	+41 2 22.12	25.252	24.771	0.654	0.509	0.5636	0.9900	0.7203
58240	0 43 19.72	+41 3 48.54	25.209	24.374	1.007	0.854	0.5100	0.7206	0.4433
98140	0 43 19.75	+41 4 18.93	25.382	24.778	0.738	0.619	0.5820	0.6530	0.4487
102938	0 43 19.79	+41 3 39.45	25.294	24.777	0.646	0.543	0.5084	1.0566	0.8253
93377	0 43 19.80	+41 2 16.94	25.229	24.734	0.571	0.506	0.5187	0.7679	0.6472
90595	0 43 19.80	+41 4 26.32	25.289	24.777	0.636	0.528	0.5622	0.7532	0.5504
77493	0 43 19.82	+41 3 35.08	25.012	24.563	0.627	0.475	0.6507	0.8930	0.6068
63547	0 43 19.83	+41 2 19.42	25.173	24.615	0.736	0.577	0.6700	0.6537	0.3963
53439	0 43 19.83	+41 4 23.49	25.007	24.447	0.750	0.589	0.5837	0.9304	0.6330
85991	0 43 19.83	+41 5 9.77	25.205	24.718	0.669	0.515	0.5428	0.9008	0.6054
52629	0 43 20.02	+41 2 9.83	25.045	24.461	0.656	0.601	0.6000	1.0736	0.9549
118554	0 43 20.05	+41 2 50.73	25.559	25.038	0.716	0.564	0.5000	1.0367	0.6813
104863	0 43 20.09	+41 3 57.66	25.459	24.920	0.537	0.539	0.5644	0.4951	0.4976
88211	0 43 20.11	+41 4 44.44	25.327	24.693	0.680	0.637	0.5953	0.3226	0.2390
109306	0 43 20.15	+41 2 8.24	25.614	24.938	0.830	0.693	0.5076	0.7617	0.5666
100504	0 43 20.17	+41 5 14.04	25.373	24.747	0.928	0.692	0.5131	1.2400	0.7046
114896	0 43 20.17	+41 4 23.67	25.499	24.999	0.584	0.512	0.4465	0.8285	0.7000
62963	0 43 20.20	+41 2 8.32	25.001	24.472	0.631	0.542	0.6532	0.7324	0.5816
89838	0 43 20.28	+41 2 43.11	25.322	24.756	0.689	0.585	0.5600	0.8024	0.5968
107923	0 43 20.29	+41 3 47.82	25.341	24.838	0.648	0.535	0.4500	1.1318	0.8857
73554	0 43 20.33	+41 4 30.70	25.168	24.653	0.690	0.553	0.4970	0.9855	0.6643
86690	0 43 20.34	+41 3 0.38	25.224	24.684	0.582	0.544	0.6552	0.5578	0.4976
83688	0 43 20.37	+41 4 28.09	25.232	24.621	0.719	0.623	0.6742	0.6865	0.5182
42737	0 43 20.41	+41 4 20.32	24.881	24.384	0.604	0.506	0.6806	0.4858	0.3202

**Table 9.** c-type RR Lyraes in Control WFC2 Field

Star ID	R. A. (J2000)	Dec (J2000)	$\langle V \rangle$	$\langle I \rangle$	$(V-I)_{min}$	$\langle V-I \rangle$	Period (days)	V Amplitude	I Amplitude
65950	0 43 18.49	+41 4 40.08	25.099	24.640	0.568	0.465	0.3337	0.3478	0.2000
103817	0 43 18.57	+41 3 7.61	25.355	24.972	0.418	0.386	0.3460	0.3824	0.3252
91215	0 43 18.78	+41 2 24.17	25.231	24.824	0.432	0.409	0.3439	0.3137	0.2731
93640	0 43 18.83	+41 4 51.84	25.347	24.807	0.634	0.547	0.3330	0.3698	0.2415
53982	0 43 18.83	+41 4 6.12	24.948	24.471	0.522	0.481	0.3692	0.2962	0.2375
91682	0 43 19.17	+41 4 34.53	25.287	24.879	0.416	0.408	0.3207	0.3438	0.3294
100571	0 43 19.19	+41 5 11.30	25.350	24.906	0.455	0.445	0.3204	0.3032	0.2883
57036	0 43 19.20	+41 5 13.52	24.938	24.448	0.554	0.495	0.4000	0.3352	0.2492
55572	0 43 19.22	+41 3 51.00	24.981	24.768	0.324	0.224	0.3456	0.4963	0.3279
61220	0 43 19.26	+41 4 33.75	25.035	24.699	0.376	0.338	0.3291	0.2597	0.2000
93071	0 43 19.44	+41 2 47.17	25.312	24.950	0.432	0.367	0.3246	0.3719	0.2661
61922	0 43 19.48	+41 4 18.85	25.091	24.680	0.483	0.417	0.3707	0.3927	0.2860
116392	0 43 19.70	+41 3 16.75	25.661	25.069	0.634	0.595	0.3580	0.4392	0.3847
53906	0 43 19.74	+41 5 9.17	24.993	24.538	0.474	0.455	0.4097	0.2946	0.2690
87001	0 43 19.80	+41 2 46.17	25.246	24.953	0.421	0.302	0.2792	0.4954	0.3015
61164	0 43 19.82	+41 5 4.55	25.112	24.511	0.724	0.610	0.3169	0.3826	0.2192
76494	0 43 19.93	+41 4 43.72	25.231	24.754	0.562	0.485	0.2600	0.4068	0.2728
87151	0 43 20.05	+41 4 38.76	25.242	24.846	0.520	0.406	0.3052	0.3963	0.2145
94952	0 43 20.12	+41 3 18.43	25.309	24.821	0.563	0.493	0.3306	0.3265	0.2292
92741	0 43 20.13	+41 5 10.20	25.249	24.889	0.361	0.360	0.3200	0.2014	0.2000
99130	0 43 20.22	+41 2 2.10	25.559	24.815	0.816	0.750	0.3557	0.4493	0.3404
107523	0 43 20.28	+41 2 23.06	25.395	24.978	0.496	0.422	0.3530	0.4005	0.2900
54458	0 43 20.32	+41 3 18.78	25.124	24.529	0.654	0.600	0.3062	0.3907	0.2981
52396	0 43 20.35	+41 3 7.58	24.957	24.510	0.586	0.459	0.3632	0.4569	0.2624
75712	0 43 20.48	+41 5 0.33	25.149	24.686	0.560	0.468	0.4237	0.3330	0.2000
38568	0 43 20.55	+41 4 39.55	24.821	24.172	0.771	0.659	0.3450	0.3689	0.2000
63693	0 43 20.58	+41 2 31.91	25.183	24.685	0.579	0.505	0.3602	0.4598	0.3514
102360	0 43 20.60	+41 2 37.34	25.406	25.010	0.406	0.396	0.3088	0.3503	0.3361
99589	0 43 20.62	+41 4 15.76	25.297	24.976	0.407	0.329	0.2649	0.4075	0.2666
92289	0 43 20.68	+41 3 40.56	25.196	24.779	0.493	0.423	0.2944	0.3799	0.2752
76548	0 43 20.71	+41 2 51.40	25.139	24.694	0.528	0.450	0.3461	0.3520	0.2386
95206	0 43 20.77	+41 5 11.83	25.338	24.904	0.522	0.440	0.2759	0.3775	0.2510
81332	0 43 20.97	+41 4 45.00	25.139	24.694	0.529	0.451	0.3659	0.3573	0.2370
99423	0 43 21.20	+41 3 54.75	25.319	24.901	0.565	0.429	0.3471	0.4301	0.2184
53824	0 43 21.24	+41 4 25.99	25.082	24.583	0.653	0.512	0.3000	0.4667	0.2536
53824	0 43 21.24	+41 4 25.99	25.082	24.583	0.653	0.512	0.3000	0.4667	0.2536
53824	0 43 21.24	+41 4 25.99	25.082	24.583	0.653	0.512	0.3000	0.4667	0.2536
75609	0 43 21.27	+41 2 47.10	25.156	24.834	0.423	0.329	0.3179	0.3561	0.2000
61020	0 43 21.32	+41 3 19.00	24.978	24.567	0.432	0.411	0.4339	0.3188	0.2843
102127	0 43 21.37	+41 3 15.27	25.312	25.076	0.295	0.240	0.2622	0.3914	0.2987
84887	0 43 21.43	+41 3 24.65	25.217	24.787	0.489	0.435	0.2820	0.4265	0.3299
86478	0 43 21.48	+41 4 26.78	25.239	24.759	0.609	0.490	0.3324	0.3801	0.2000
89379	0 43 21.57	+41 5 11.50	25.232	24.849	0.414	0.385	0.3263	0.3470	0.2921
98001	0 43 21.64	+41 3 38.30	25.263	24.898	0.456	0.372	0.2883	0.4130	0.2737
92458	0 43 21.69	+41 3 21.96	25.269	24.907	0.471	0.370	0.2760	0.4039	0.2385
78776	0 43 21.74	+41 5 20.35	25.201	24.690	0.601	0.518	0.3700	0.3468	0.2293
94673	0 43 21.86	+41 4 59.02	25.284	24.925	0.440	0.364	0.3173	0.3244	0.2004
102263	0 43 21.95	+41 3 45.05	25.287	24.970	0.369	0.321	0.2900	0.3290	0.2487
71607	0 43 21.99	+41 2 28.70	25.037	24.690	0.344	0.347	0.3225	0.2304	0.2342
78085	0 43 22.04	+41 2 38.35	25.176	24.807	0.449	0.375	0.3395	0.3550	0.2359
114415	0 43 22.15	+41 4 17.44	25.497	25.144	0.419	0.357	0.2725	0.3577	0.2478
90590	0 43 22.28	+41 2 30.57	25.180	24.827	0.403	0.357	0.2919	0.3758	0.2898
63996	0 43 22.33	+41 3 11.16	24.997	24.631	0.473	0.377	0.3228	0.4892	0.3065
70542	0 43 22.35	+41 4 38.65	25.095	24.735	0.403	0.364	0.3373	0.4026	0.3300
100201	0 43 22.35	+41 5 16.87	25.377	24.984	0.447	0.398	0.2840	0.4326	0.3495
74815	0 43 22.36	+41 3 45.92	25.122	24.609	0.488	0.512	0.4274	0.2347	0.2683
85472	0 43 22.38	+41 3 11.73	25.140	24.731	0.512	0.416	0.3041	0.3610	0.2166
88939	0 43 22.47	+41 4 59.05	25.186	24.765	0.562	0.431	0.3745	0.3947	0.2000
98433	0 43 22.70	+41 3 54.38	25.349	25.018	0.442	0.342	0.3100	0.5076	0.3388
82255	0 43 22.76	+41 4 38.08	25.138	24.785	0.434	0.359	0.3000	0.4114	0.2831
98244	0 43 22.86	+41 3 33.92	25.289	24.873	0.460	0.419	0.3381	0.3600	0.2946
95595	0 43 22.90	+41 3 3.47	25.227	24.815	0.467	0.416	0.3075	0.3951	0.3132
90668	0 43 22.94	+41 4 24.06	25.198	24.885	0.387	0.320	0.3000	0.3894	0.2774
86753	0 43 23.22	+41 2 7.28	25.233	24.912	0.427	0.330	0.3192	0.4457	0.2793
92751	0 43 23.27	+41 4 42.69	25.169	24.817	0.464	0.363	0.3148	0.5265	0.3610
81133	0 43 23.27	+41 4 32.46	25.118	24.756	0.401	0.365	0.3656	0.3319	0.2707

**Table 10.** Results of the Light Curve Simulations

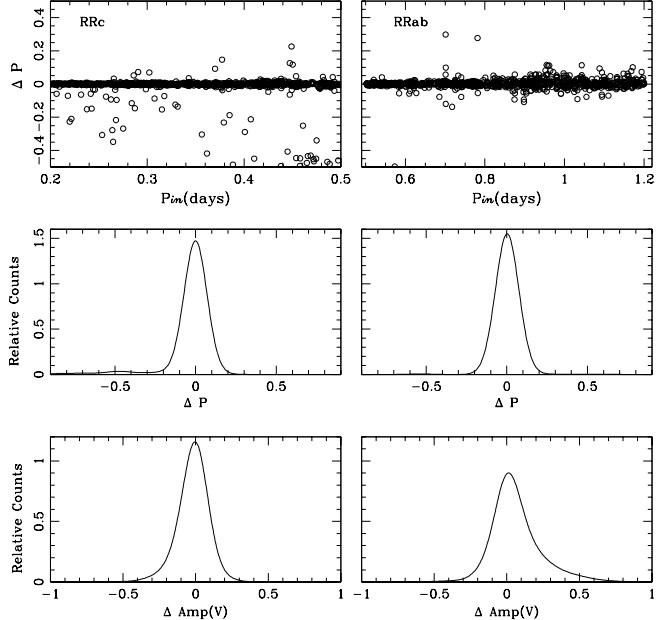
Field	RR Lyrae type	Period Error	Amplitude Error	Percent Within $\pm 0.05d$	Percent Within $\pm 0.1d$
M32	RRab	$\pm 0.0014$	$\pm 0.0084$	83%	96%
M32	RRc	$\pm 0.0104$	$\pm 0.0061$	79%	81%
Control	RRab	$\pm 0.0008$	$\pm 0.0055$	94%	98%
Control	RRc	$\pm 0.0044$	$\pm 0.0046$	91%	94%

**Figure 5.** The results of our RR Lyrae light curve simulations using an observing cadence appropriate for the M32 field.

to M32. This can be compared with the results of Fiorentino et al. (2012), who claimed a total of 83 RR Lyraes belonging to M32 in this field. The difference between these two estimates likely stems from two sources. First, we have identified and characterized 509 RR Lyraes in the M32 field compared with 416 from Fiorentino et al. (2012) – a factor of 1.22 more objects. Second, the background density of M31 RR Lyraes in the present paper is approximately a factor of 1.4 lower than that assumed by Fiorentino et al. (2012) – 0.0077 stars/sq arcsec compared with 0.011 stars/sq arcsec. If we use the background density adopted by Fiorentino et al. (2012), we arrive at a total number of 71 RR Lyraes belonging to M32, which, when multiplied by a factor of 1.22, yields 87 RR Lyraes, which is close to the value of 83 quoted by Fiorentino et al. (2012). As a result, the main source of the difference between the present work and that of Fiorentino et al. (2012) with regard to the number of RR Lyraes belonging to M32 is the adopted contribution of such stars from the M31 background.

## 5.2 The Bailey Diagram of RR Lyrae Variables Associated with M32

Figure 10 shows the Bailey Diagrams for the RR Lyraes in the M32 field. The ab-type RR Lyraes are shown by the filled

**Figure 6.** The results of our RR Lyrae light curve simulations using an observing cadence appropriate for the Control field.

points while the c-type variables are plotted as open circles. The Oosterhoff I and II loci are also indicated (Clement & Rowe 1999). A comparison of these diagrams with Fig. 10 of S09 suggests that the RR Lyraes in the M32 field are located slightly to the left (shorter period) of the Oosterhoff I line. We note that this field has no significant population of Oosterhoff II RR Lyraes. We return to this point in Section 6.1 below.

For the sake of completeness, we note that the mean periods of the RR Lyraes in the M32 field are  $\langle P_{ab} \rangle = 0.575 \pm 0.004$  (sem) d and  $\langle P_c \rangle = 0.326 \pm 0.005$  (sem) d. These are to be compared with mean periods of  $\langle P_{ab} \rangle = 0.559$  d and  $\langle P_c \rangle = 0.326$  d for the Oosterhoff I Galactic globular clusters (Jeffery et al. 2011).

## 5.3 The Metallicity of RR Lyrae Variables Associated with M32

We can calculate the metallicities of ab-type RR Lyraes in two ways. Using the data of Layden (2005, private communication) for 132 Galactic RR Lyraes in the solar neighborhood, Sarajedini et al. (2006) established a relation between period and metal abundance of the form

$$[\text{Fe}/\text{H}] = -3.43 - 7.82 \log P_{ab}. \quad (1)$$

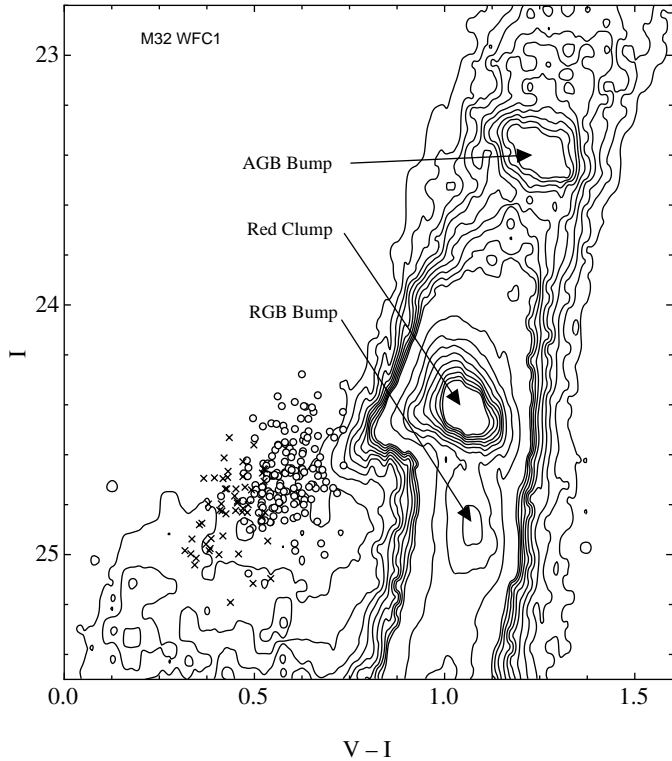


**Figure 7.** The color-magnitude diagram (CMD) of stars measured on the WFC1 chip of the M32 field. The ab-type RR Lyraes are indicated as open circles while the c-types are shown as crosses.

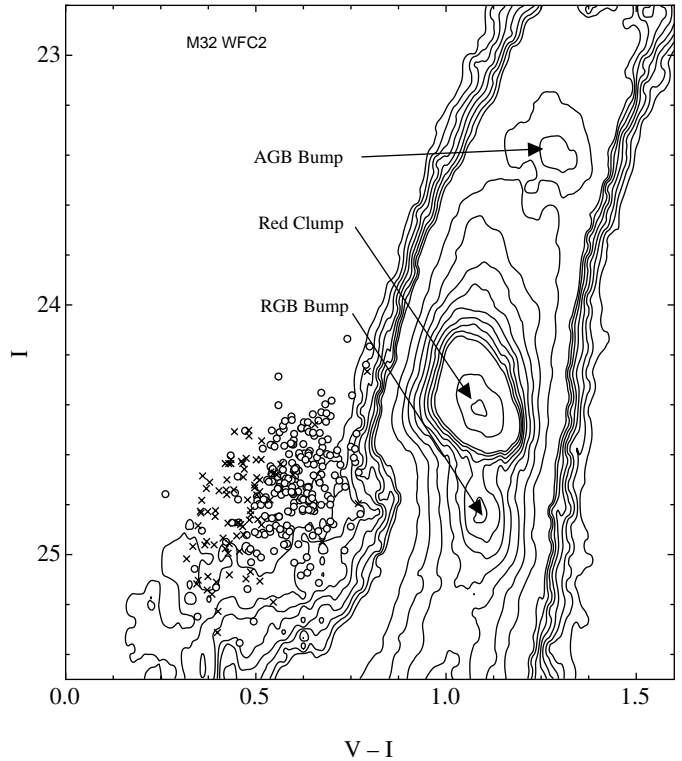


**Figure 8.** The color-magnitude diagram (CMD) of stars measured on the WFC2 chip of the M32 field. The ab-type RR Lyraes are indicated as open circles while the c-types are shown as crosses.

This equation does not take into account the amplitudes of the RR Lyraes even though, as the Bailey Diagrams show, there is a relation between amplitude and period for the ab-types. Including this effect, Alcock et al. (2000) gave a period-amplitude-metallicity relation of the form

$$[\text{Fe}/\text{H}] = -8.85[\log P_{ab} + 0.15A(V)] - 2.60, \quad (2)$$

where  $A(V)$  represents the amplitude in the  $V$ -band. S09 suggest that if the amplitudes of the RR Lyraes are well-determined, then equation (2) yields more precise metal abundances than equation (1). As a result, we will use equation (2) exclusively for the remainder of this paper.

For the 375 RRab stars in the M32 field, the solid line in Fig. 11 shows the distribution of  $[\text{Fe}/\text{H}]$  values given by equation (2). We find an average metal abundance of  $\langle [\text{Fe}/\text{H}] \rangle = -1.42 \pm 0.02$  (sem) dex for these M32 RR Lyraes. The dashed line in Fig. 11 illustrates the metallicity distribution from Field 1 of S09, which is dominated by M31 RR Lyraes, where the average turns out to be  $\langle [\text{Fe}/\text{H}] \rangle = -1.46 \pm 0.03$  (sem) dex. Furthermore, Fiorentino et al. (2010) find an average metallicity of  $\langle [\text{Fe}/\text{H}] \rangle = -1.52 \pm 0.10$  dex in their F1 field, which is contained within our M32 field. These three average values are statistically indistinguishable to within the errors. We note also that we investigated the presence of a radial metallicity gradient among the RR Lyraes in M32 but found no evidence supporting such a gradient.

#### 5.4 The Reddening and Distance to M32

The work of Guldenschuh et al. (2005) showed that the minimum light color of ab-type RR Lyrae variables is equal to  $V - I = 0.58 \pm 0.02$  mag regardless of their metal abundances and pulsation properties such as period and amplitude. Given this fact, we can calculate the reddening for each RRab variable in our sample as shown in Fig. 12. The Gaussian curve is fitted to the M32 Field RR Lyraes and shows that the shape of the reddening histogram is consistent with a Gaussian distribution. The error on any given reddening value is composed of  $\pm 0.02$  mag from the Guldenschuh et al. (2005) calibration and  $\pm 0.05$  mag from the uncertainty inherent in the measurement of the minimum light colors. This latter value is taken from the results of our synthetic light curve simulations described above. Taken together, these two errors suggest that the majority of the dispersion in the reddening distribution is attributable to errors inherent in the measurement of the RR Lyrae minimum light color as opposed to internal reddening due to M31 and/or M32. The mean reddening for the ab-type RR Lyraes in the M32 field is  $\langle E(V - I) \rangle = 0.134 \pm 0.088$  (sdm)  $\pm 0.005$  (sem) mag. We note that the Schlegel, Finkbeiner & Davis (1998) dust maps suggest a line-of-sight reddening to M32 of  $E(B - V) = 0.08$  mag, which translates to  $E(V - I) = 0.11$  mag (Tammann, Sandage & Reindl 2003). This is consistent with our mean  $E(V - I)$  values based on the minimum light colors of the ab-type RR Lyraes thereby corroborating the findings of previous investigators that M32 is largely free of interstellar

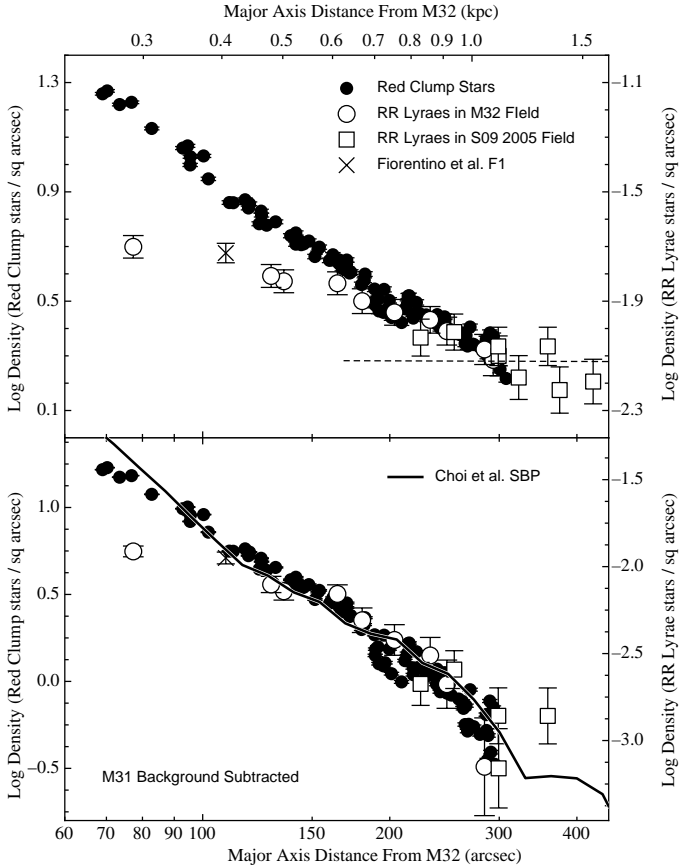


**Figure 9.** The radial density profiles of red clump stars and RR Lyrae variables projected along the major axis of M32. The upper panel shows the raw profiles corrected for photometric incompleteness before the subtraction of the M31 background. In addition to the red clump stars (filled circles) and RR Lyraes (open circles) from the present study, we also include the RR Lyraes from the Fiorentino et al. (2010, cross) F1 HRC field and from Field 1 of S09 (open squares). The profiles of these two populations have been scaled to match in the region outside of 150 arcsec. The upper abscissa assumes a M32 distance of 770 kpc. The lower panel, we have subtracted the M31 background density from the red clump stars and RR Lyraes and also include the M32 major axis surface brightness profile (SBP) from Choi et al. (2002) scaled to fit the red clump and RR Lyrae distribution.

dust (Ford et al. 1978; Impey et al. 1986; Lauer et al. 1998; Corbin et al. 2001; Choi et al. 2002).

With a determination of the line of sight reddening and the mean metallicity of the ab-type RR Lyrae variables, we can now calculate the distance to M32. We use the RR Lyrae luminosity–metallicity relation of Chaboyer (1999):  $M_V(RR) = 0.23[\text{Fe}/\text{H}] + 0.93$  mag. Adopting  $E(B - V) = 0.08 \pm 0.03$  mag and  $\langle [\text{Fe}/\text{H}] \rangle = -1.42 \pm 0.20$  (zeropoint error in the abundance scale) dex, along with  $\langle V(\text{RR}) \rangle = 25.28 \pm 0.05$  (zeropoint error from Sirianni et al. 2005) mag, we find  $\langle (V - M)_o \rangle = 24.42 \pm 0.12$  mag for the distance to M32. This distance is consistent with a number of previous authors:  $24.55 \pm 0.08$  mag (Tonry et al. 2001),  $24.39 \pm 0.08$  mag (Jensen et al. 2003), and  $24.53 \pm 0.12$  mag (Monachesi et al. 2011).

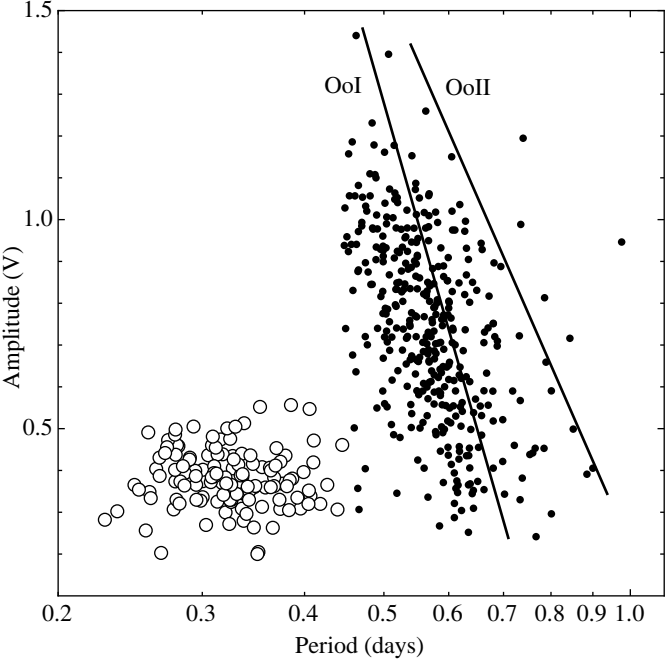


**Figure 10.** The Bailey Diagram for the RR Lyraes in the M32 field showing V amplitude on the ordinate and period in days on the abscissa. The filled circles represent the ab-type RR Lyraes while the open circles are the c-types. The loci of ab-type RR Lyraes in Oosterhoff I and II Galactic globular clusters from Clement & Rowe (1999) are also shown.

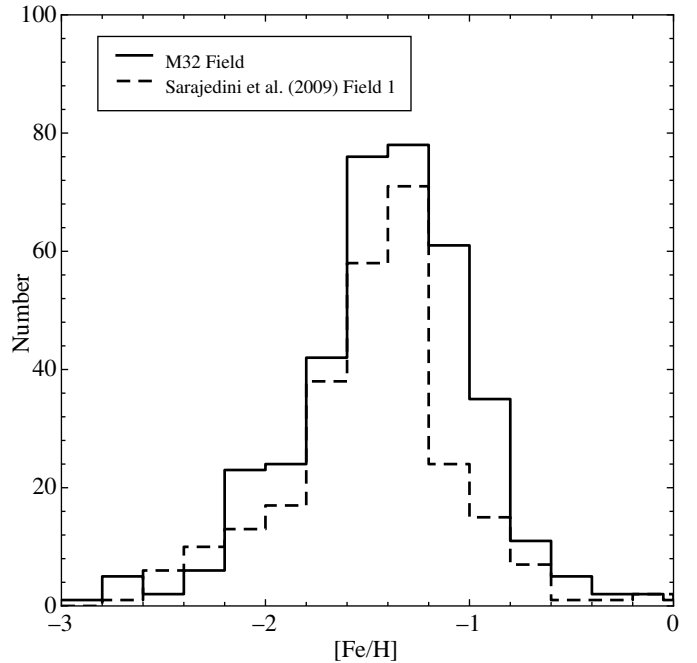


**Figure 11.** The distribution of metallicities calculated using the equation from Alcock et al. (2000). The solid line represents ab-type RR Lyraes in our M32 Field while the dashed line is based on the field 1 RR Lyraes from S09.

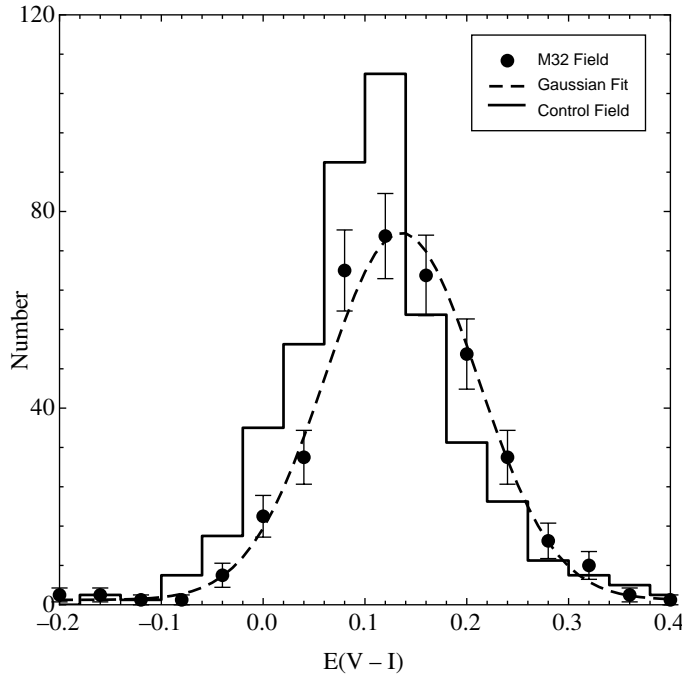


**Figure 12.** The distribution of reddening calculated from the ab-type RR Lyrae in the M32 and control fields. The dashed line is the Gaussian fit to the points.

### 5.5 The Specific Frequency of M32 RR Lyraes and the Ancient Metal-Poor Population of M32

We now compute the specific frequency of RR Lyrae stars in M32. With this number we can hope to understand the ancient, metal-poor population in M32 in the context of Galactic globular clusters. Suntzeff, Kinman & Kraft (1991) define the specific frequency of RR Lyrae stars  $S_{RR}$  as the number of RR Lyrae stars  $N_{RR}$  per unit luminosity, normalized to a typical Galactic globular cluster luminosity of  $M_{Vt} = -7.5$  mag:

$$S_{RR} = N_{RR}/10^{-0.4(M_{Vt}+7.5)} \quad (3)$$

(following the notation of Harris 1996).

In order to compute  $S_{RR}$  for M32 RR Lyrae variables, we need to determine the luminosity of old, metal-poor M32 stars contained in the M32 ACS/WFC field. We first compute the total  $B$ -band magnitude of M32 in this field by integrated the  $B$ -band surface brightness profile of Choi et al. (2002) within the ACS/WFC field; this gives  $B = 11.85$  mag. The average color of M32 beyond one effective radius is  $(B - V) = 0.88$  mag (de Vaucouleurs et al. 1991), so  $V = 10.97$  mag. Combined with the distance modulus and extinction (assuming  $A_V/E(B - V) = 3.315$ , Schlegel et al. 1998) determined in the previous section, we find that the total  $V$ -band luminosity in the M32 field is  $M_{Vt} = -13.7$ . Monachesi et al. (2011) determined an upper limit of  $\approx 4.5\%$  of M32's mass was contained in stars with  $[Fe/H] < -1$ , or a total of  $\approx 5.5\%$  of the  $V$ -band light from an analysis of the CMD of the RGB; Monachesi et al. (2012) determined a lower limit of  $\approx 1\%$  of M32's mass was contained in similarly metal-poor stars from analysis of the CMD near the (young) main-sequence turnoffs, or a total of  $\approx 1.3\%$  of the  $V$ -band

light. We use these two values as bounds on the ancient, metal-poor starlight in the M32 ACS/WFC field; these correspond to  $M_{Vt} \approx -10.6$  mag (upper limit) and  $M_{Vt} \approx -9.0$  mag (lower limit) in this population. Using these luminosities, we finally derive  $13 \lesssim S_{RR} \lesssim 56$  for M32's RR Lyrae population (for the upper and lower limits to the mass of the ancient, metal-poor stars in M32, respectively). The lower limit is a factor of two larger than the value found in the much smaller ACS/HRC field by Fiorentino et al. (2010) due to our assumption of a smaller fraction of metal-poor light than assumed in that paper (5.5% versus 11%; the larger fraction was based on a preliminary analysis of the ACS/HRC data presented in Monachesi et al. 2011). On the other hand, the range of possible values falls within the range of Galactic globular clusters: Brown et al. (2004) find that  $1 \lesssim S_{RR} \lesssim 50$  at  $[Fe/H] \approx -1.4$  dex for Galactic globular clusters using the data presented in Harris (1996).

As discussed in Fiorentino et al. (2010), the large dispersion in  $S_{RR}$  in Galactic globular clusters with  $[Fe/H] < -1$  dex (due to the “second-parameter problem”) means that there is no way to invert this relation to determine the *true* fraction of ancient, metal-poor stars in a population; nor do there appear to be stellar evolution models currently available that predict the population of RR Lyrae *a priori* (see, e.g., Salaris & Cassisi 2005). The presence of RR Lyrae variables tells us that ancient, metal-poor stars are *definitely* present in M32 – a result that cannot be clearly demonstrated by existing CMDs of M32 (e.g., Monachesi et al. 2011; Monachesi et al. 2012). This in itself is a very useful result, of course, as it shows that at least some phase of M32's evolution included metal-poor stars (Fiorentino et al. 2010, 2012).

### 5.6 Comparison with Previous Studies

The work of Fiorentino et al. (2010) imaged a field approximately 1.8 arcmin from the center of M32, which is wholly contained within the M32 field analyzed herein. They found 17 RR Lyrae in their HRC field of which 13 are recovered in our photometry. These numbers are not unexpected given the fact that our photometric completeness at this location is 88% compared to 100% for the Fiorentino et al. (2010) study. We have matched the RR Lyrae in common and compared the derived periods, amplitudes, and magnitudes. For the periods, there is a mean difference of  $\langle \Delta P \rangle = -0.0017 \pm 0.0048$  (sem) days in the sense (Fiorentino–Us). In the case of the RR Lyrae amplitudes, we have adjusted for the difference in amplitudes expected in the F555W (Fiorentino et al. 2010) and F606W filters (Present Work) by decreasing the latter by 8%, based on the work of Brown et al. (2004) and S09. After making this adjustment, we calculate a difference of  $\langle \Delta \text{Amp}(V) \rangle = 0.016 \pm 0.035$  (sem). The mean V magnitude difference is  $\langle \Delta V \rangle = 0.016 \pm 0.029$  (sem), again in the sense (Fiorentino–Us). We see that all of these differences are quite small and well within the quoted errors.

In the case of the Fiorentino et al. (2012) RR Lyrae sample, they do not provide tables of RR Lyrae data in their paper; however, we can compare the mean properties of these stars between our study and theirs. For example, Fiorentino et al. (2012) find  $\langle P_{ab} \rangle = 0.55 \pm 0.07$  (sdm) and  $\langle P_c \rangle = 0.32 \pm 0.04$  (sdm). In the case of the present study,

our analysis yields  $\langle P_{ab} \rangle = 0.575 \pm 0.004$  (sem) and  $\langle P_c \rangle = 0.326 \pm 0.005$  (sem). The average periods of the ab-type and c-type RR Lyraes are in good accord between the two studies. In addition, Fiorentino et al. (2012) quote a mean intrinsic  $V$  magnitude of  $\langle V_o \rangle = 24.95 \pm 0.18$  mag. Given their adopted reddening of  $E(B-V) = 0.08$ , this translates to a mean apparent magnitude of  $\langle V(RR) \rangle = 25.20$ , which is in agreement with our value of  $\langle V(RR) \rangle = 25.30 \pm 0.05$ .

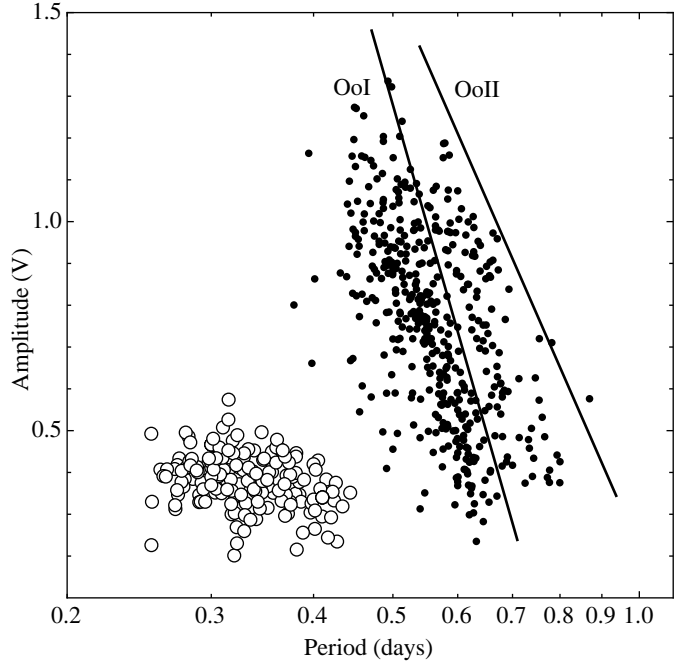
## 6 RR LYRAE VARIABLES IN M31

We now turn to the properties of RR Lyrae variables in M31, concentrating on the Control field and its implications for the M31 spheroid.

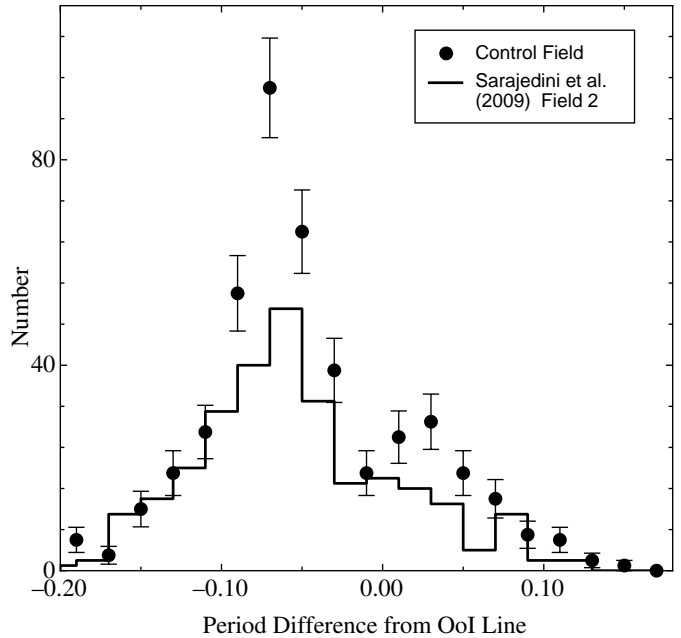
### 6.1 The Bailey Diagram of M31 RR Lyrae Variables

Figure 13 shows the Bailey Diagram for the RR Lyraes in the Control field (see Fig. 10 for the M32 population). In contrast to the M32 field, the RR Lyraes in the Control field reveal an intriguing bimodal appearance with two distinct ab-type sequences roughly bisected by the Oosterhoff type I locus. This is the first time that such bimodal behavior has been observed among the field RR Lyrae population of M31. We investigate the significance of this phenomenon in the following sections. For now, we note, as for M32, this field does not have a significant population of Oosterhoff II RR Lyraes. As noted by S09 and Yang & Sarajedini (2012), this further underscores the general dearth of Oosterhoff II RR Lyraes in the spheroid of M31. In fact, almost all of the M31 fields observed so far – except for the Control field considered here – and M32 exhibit Bailey Diagrams that resemble each other, i.e., they are all aligned with or slightly offset to shorter periods compared with the Oo I line. For completeness, we find  $\langle P_{ab} \rangle = 0.568 \pm 0.004$  (sem) d and  $\langle P_c \rangle = 0.333 \pm 0.003$  (sem) d for the Control field.

In order to investigate the robustness of the bimodality in Fig. 13, we take each ab-type RR Lyrae in the Bailey Diagram and calculate its period difference relative to the Oosterhoff I line shown in Fig. 13. Since the Oosterhoff I locus roughly bisects the two subpopulations as noted above, it is a natural fiducial for this purpose. The resultant histogram of period differences is shown as the filled points in Fig. 14 wherein the solid line histogram is the Field 2 data from Sarajedini et al. (2009). The latter distribution has been shifted horizontally by  $-0.03$  d in order to match the dominant peaks of the two histograms so that they can be compared in a relative manner. We see that the secondary peak present in the Control field histogram is not present in field 2 of Sarajedini et al. (2009). It is also possible to compare the control field histogram shown in Fig. 14 with a single-peaked Gaussian distribution with the same mean and standard deviation via the Kolmogorov-Smirnov (K-S) test. We find that there is only a 1% chance that the two distributions are from the same parent population. This suggests that the bimodal appearance of the Control field Bailey Diagram is likely to be genuine.



**Figure 13.** The Bailey Diagram for the RR Lyraes in the Control field showing  $V$  amplitude on the ordinate and period in days on the abscissa. The filled circles represent the ab-type RR Lyraes while the open circles are the c-types. The loci of ab-type RR Lyraes in Oosterhoff I and II Galactic globular clusters from Clement & Rowe (1999) are also shown.



**Figure 14.** The filled circles represent the histogram of period differences for each ab-type RR Lyrae in the Control field relative to the Oosterhoff I line shown in Fig. 13. The solid line is the histogram of period differences measured in the same way for the ab-type RR Lyraes in Field 2 of Sarajedini et al. (2009). The latter has been shifted horizontally by  $-0.03$  d in order to match the dominant peaks of the two histograms.

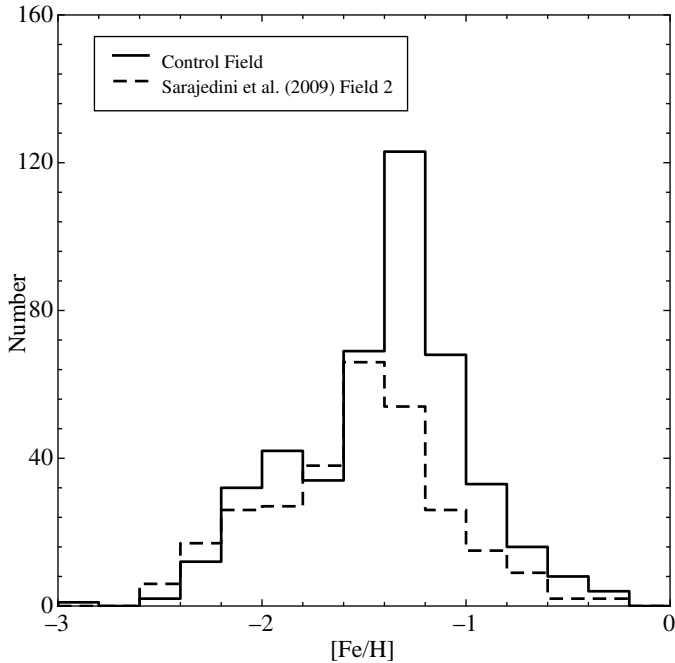


**Figure 15.** The distribution of metallicities calculated using the equation from Alcock et al. (2000). The solid line represents ab-type RR Lyrae stars in our Control Field while the dashed line is based on the field 2 RR Lyrae stars from S09.

## 6.2 The Metallicities of M31 RR Lyrae Variables

Following the analysis of Section 5.3 above, the metallicity distribution function of the 446 ab-type RR Lyrae stars in the Control field is shown in Fig. 15. Not surprisingly, given the bimodal appearance of the Bailey Diagram, these RR Lyrae stars exhibit a bimodal metallicity distribution with a well-pronounced peak at  $[Fe/H] \approx -1.3$  dex and another at  $[Fe/H] \approx -1.9$  dex. This is in contrast to the single peaked distributions of the M32 field and all previous M31 fields published to date (e.g. S09; Fiorentino et al. 2010; Jeffery et al. 2011). Figure 15 compares the Control field MDF with that of the RRab stars in field 2 from S09, which has a mean abundance of  $\langle [Fe/H] \rangle = -1.54 \pm 0.03$  (sem) dex. Upon closer examination, it would appear that the latter may exhibit a metal-poor tail that corresponds to the metal-poor peak shown by the Control field. In any case, the bimodal appearance of Figs. 14 and 15 suggest that the Control field line-of-sight intersects two old stellar populations with distinctly different mean metallicities. It is possible that the primary peak represents a stellar population belonging to the putative M31 spheroid while the more metal-poor population could have originated in a disrupted M31 dwarf satellite galaxy. If so, then the bimodal appearance of Fig. 13 represents more evidence supporting the merger and accretion history of the M31 spheroid (McConnachie et al. 2009).

## 6.3 The Reddening and Distance to M31

Following the discussion in Section 5.4, we find for the Control field an average reddening of  $\langle E(V-I) \rangle = 0.111 \pm 0.088$  (sdm)  $\pm 0.004$  (sem) mag (see Fig. 12). Using this value and a mean metallicity of  $\langle [Fe/H] \rangle = -1.39 \pm 0.20$  dex for the

Control field, we find a mean magnitude of the RR Lyrae stars in this field of  $\langle V(RR) \rangle = 25.27 \pm 0.05$  mag. Once again adopting  $E(B-V) = 0.08 \pm 0.03$ , we infer a distance modulus of  $\langle (V-M)_o \rangle = 24.41 \pm 0.12$  mag, which is in agreement with the result from the M32 field. We can also proceed slightly differently here by dividing the ab-type RR Lyrae stars in the Control field at  $[Fe/H] = -1.7$  dex and calculating the distance for each group separately. We find that those with  $[Fe/H] < -1.7$  dex exhibit a distance modulus of  $\langle (V-M)_o \rangle = 24.43 \pm 0.12$  mag while those with  $[Fe/H] \geq -1.7$  dex have  $\langle (V-M)_o \rangle = 24.41 \pm 0.12$  mag. These are essentially the same indicating that, to the level of precision with which we are able to measure it, the two stellar population components in the Control field are at the same distance. Furthermore, our distances are consistent with a number of previous values for the true distance modulus of M31, e.g.  $24.44 \pm 0.11$  mag (Freedman & Madore 1990),  $24.50 \pm 0.10$  mag (Brown et al. 2004), and  $24.47 \pm 0.07$  mag (McConnachie et al. 2005).

## 6.4 RR Lyraes in the M31 Spheroid

We can gain insight into the broader properties of RR Lyrae stars in M31 by examining the radial distribution of the RR Lyrae populations thus far studied. Figure 16 illustrates these data wherein the top panel shows the radial density distribution of M31 RR Lyrae stars compared with three M31 minor axis surface brightness profiles. The two inner data points come from S09 where ‘halo4’ represents their Field 2 and ‘halo6’ is their Field 1. The points designated ‘M32’ and ‘Control’ are from the present work. The halo11, halo21, halo35a, and halo35b fields are the minor axis fields taken from the work of Jeffery et al. (2011), while the stream and disk points also come from Jeffery et al. (2011). The warp and outer disk fields are from the paper by Bernard et al. (2012). Next to each point, we indicate the number of RR Lyrae stars at that location. All of these data are based on studies that have used HST/ACS/WFC in order to identify and characterize the RR Lyrae variables. The solid line is the minor axis surface brightness profile from Pritchett & van den Bergh (1994, see also Brown et al. 2008) scaled to match the inner two points from S09 and the outer halo points (halo21, halo35a, halo35b). Also plotted are the minor axis surface brightness profiles from Irwin et al. (2005, thin solid line) and Gilbert et al. (2009, filled squares). We see that these three profiles agree well with each other. In order to be consistent with the minor axis surface brightness profiles, the radial positions of the inner three M31 RR Lyrae fields have been projected onto the minor axis of M31 and are plotted as such. The halo11, halo21, halo35a, and halo35b points are already along the M31 minor axis.

From the top panel of Fig. 16, we note that, not surprisingly, the surface density of RR Lyrae variables in M31 drops with distance from its center. The minor axis points (halo4, halo6, halo11, halo21, halo35a, halo35b) more or less follow the plotted surface brightness profile to within the errors. The stream, disk, outer disk, and warp fields fall above the halo distribution suggesting that they are enhanced in RR Lyrae stars above what would be expected from the halo alone. This is consistent with the conclusions of Jeffery et al. (2011) and Bernard et al. (2012) that these RR Lyrae stars are genuine members of these subsystems. If this is the case,

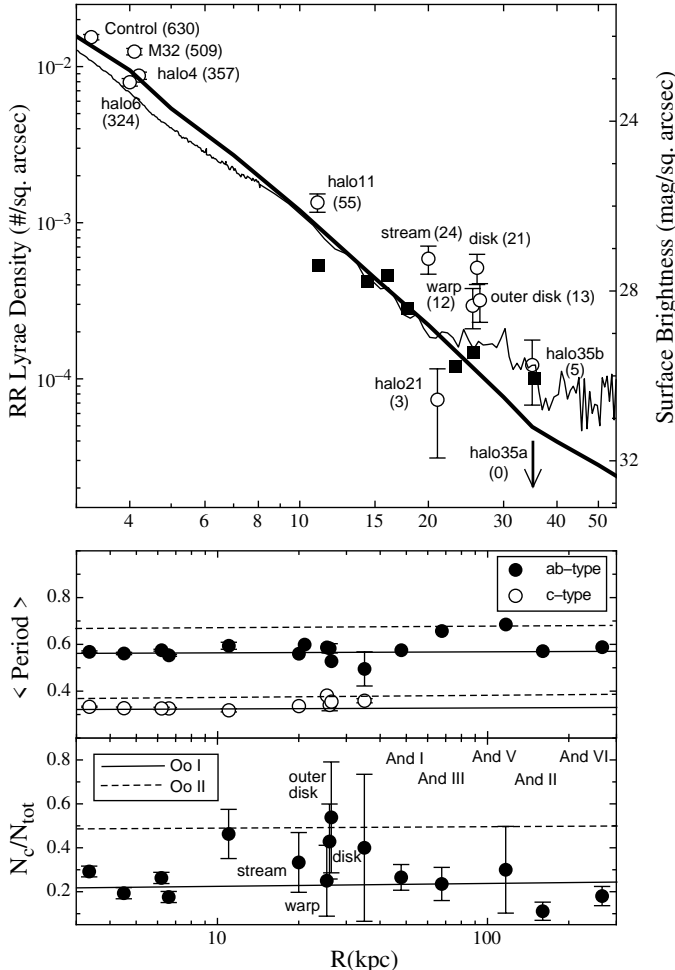


**Figure 16.** The upper panel shows the radial density profile of RR Lyraes in the spheroid of M31. These are referenced to the left ordinate scale. The solid line is the minor axis surface brightness profile from Pritchett & van den Bergh (1994, see also Brown et al. 2008 and Courteau et al. 2011) referenced to the right ordinate axis. Also plotted are the minor axis radial brightness profiles from Irwin et al. (2005, thin solid line) and Gilbert et al. (2009, filled squares). The middle panel displays the radial trend of the mean period for the ab-type (solid circles) and c-type (open circle) RR Lyrae variables. The bottom panel is similar to the middle one except that the ratio of c-type to all RR Lyraes is illustrated as a function of radial location in the M31 spheroid. The solid lines illustrate the properties of RR Lyraes in Oosterhoff I clusters while the dashed lines are for Oosterhoff II clusters. The properties of the Andromeda dwarf galaxies are taken from Table 5 of Clementini (2010). See text for more details.

then the stream, disk, outer disk, and warp of M31 harbor an old stellar population suggesting that the earliest epoch of star formation in all of these subsystems occurred at approximately the same time.

The middle panel of Fig. 16 shows the variation of mean RR Lyrae period with distance from the center of M31 for the fields shown in the top panel as well as the data for five of the dwarf spheroidal companions of M31 taken from Clementini (2010). The mean periods of Oosterhoff I and II Galactic globular clusters are also shown as solid and dashed lines, respectively, for comparison. The upper set of solid/dashed

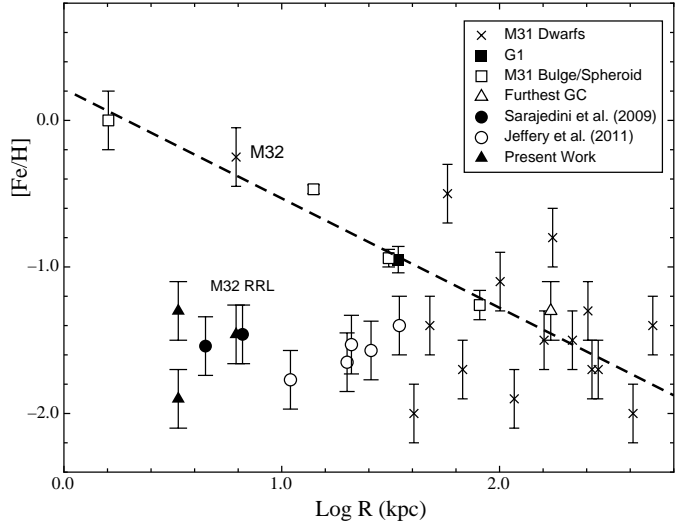


**Figure 17.** The radial variation of metal abundance in the M31 spheroid as originally presented by Sarajedini et al. (2009, filled circles) augmented by the results of the present work (filled triangles) and those of Jeffery et al. (2011, open circles). The innermost open square represents the bulge abundance measured by Sarajedini & Jablonka (2005). The remaining open squares are the bulge/halo points from the work of Kalirai et al. (2006). The dashed line is the least squares fit to these data with a slope of  $-0.75 \pm 0.11$ . The crosses represent the dwarf galaxies surrounding M31 from the work of Grebel et al. (2003) and Koch & Grebel (2006) whereas the abundance of M32 is taken from Grillmair et al. (1996). The filled square is the well-known massive globular cluster G1 studied by Meylan et al. (2001). The open triangle is the furthest known globular cluster in M31 discovered by Martin et al. (2006). All of these points have been scaled to an M31 distance of  $(m - M)_0 = 24.43$ .

lines refer to ab-type variables while the lower set are for c-type variables. These lines come from the work of Jeffery et al. (2011). We see in this diagram, that, with the exception of And III and And V, the rest of the M31 halo is solidly of Oosterhoff I type in terms of the mean periods of the RR Lyrae variables.

The bottom panel of Fig. 16 is similar to the middle panel except that the ratio of c-type to all RR Lyraes is plotted as a function of galactocentric distance. Once again, the M31 fields in the upper panel are included as well as the dwarf satellites from Clementini (2010). The conclusion we reached from the middle panel is also largely unchanged – to within the error bars, the M31 halo is best described as containing RR Lyraes that are most similar to Oosterhoff I Galactic globular clusters.

The reason that Oosterhoff I RR Lyraes dominate the M31 halo is related to the variation of metal abundance with radial position as discussed in S09. Figure 17 shows an updated version of Fig. 14 from S09. The metallicities for the RR Lyraes in the two fields considered herein are shown by the filled triangles while the open circles represent the RR Lyraes considered in the study of Jeffery et al. (2011). The inner-most point is the bulge metallicity from the work of Sarajedini & Jablonka (2005), while the remaining open squares are the bulge/halo points from the work of Kalirai et al. (2006) as shown in their Table 3. The dashed line

is the least squares fit to the open squares with a slope of  $-0.75 \pm 0.11$ . The other points represent the dwarf spheroidal companions to M31 (crosses, Grebel et al. 2003; Koch & Grebel 2006), the globular cluster G1 (filled square, Meylan et al. 2001), and the furthest globular cluster in M31 (open triangle, Martin et al. 2006). Note that we have adopted the mean metallicity of M32 from the work of Grillmair et al. (1996). All of the non-RR Lyrae metallicities are based on the colors of RGB stars save for those from the study of Grillmair et al. (1996), which utilize integrated spectral indices. All of these values are based on a distance of  $(m - M)_o = 24.43$  (770 kpc) for M31. In cases where an error in the metallicity is not available, we have adopted a value of  $\pm 0.2$  dex.

Metal abundance is the primary parameter affecting horizontal branch (HB) morphology among the Galactic globular clusters; this is also true in terms of the Oosterhoff dichotomy. As shown in Table 2 of Clementini (2010), Oosterhoff I clusters have  $[Fe/H] \approx -1.4$  while those of Oosterhoff II have  $[Fe/H] \approx -2.0$ . As Fig. 17 reveals, the halo of M31 ( $R_{gc} \gtrsim 50$  kpc) has a mean metallicity that is closer to  $[Fe/H] \approx -1.4$  than  $[Fe/H] \approx -2.0$ , thus corroborating its Oosterhoff I nature.

## 7 SUMMARY AND CONCLUSIONS

We have presented HST/ACS observations of two fields – one that samples the stellar populations of M32 and another dubbed ‘Control’ that is dominated by the spheroid of M31. Our photometry in these fields has facilitated the identification and characterization of 1139 RR Lyrae variables of which 821 are ab-type and 318 are c-type. Based on an analysis of the periods, amplitudes, magnitudes, and spatial distributions of these stars, we draw the following conclusions.

1. We find a radial gradient in the density of RR Lyraes relative to the center of M32. This gradient is consistent with the surface brightness profile of M32 suggesting that a significant number of the RR Lyraes in this region belong to M32. This provides further confirmation that M32 contains an ancient stellar population formed around the same time as the oldest population in M31 and the Milky Way.
2. The ab-type RR Lyraes in M32 are closer to the Oosterhoff I line in the Bailey Diagram as compared to the Oosterhoff II locus exhibiting a mean metal abundance of  $\langle [Fe/H] \rangle = -1.42 \pm 0.02$  (sem) dex.
3. The mean reddening we measure for the M32 RR Lyraes is consistent with being due entirely to extinction within the Milky Way reinforcing the finding of previous investigators that M32 contains little or no dust. Adopting a mean reddening of  $E(B - V) = 0.08 \pm 0.03$  mag, and a relation between RR Lyrae luminosity and metallicity, we find an absolute distance modulus of  $\langle (V - M)_o \rangle = 24.42 \pm 0.12$  mag for M32 and  $\langle (V - M)_o \rangle = 24.41 \pm 0.12$  mag for M31 based on the Control field RR Lyrae variables.
4. In the Control field, the Bailey Diagram shows the unprecedented signature of two sequences among the ab-type

RR Lyraes. When interpreted in terms of metal abundance, the primary sequence corresponds to a population of RR Lyraes with  $[Fe/H] \approx -1.3$  dex while the secondary peak occurs at  $[Fe/H] \approx -1.9$  dex. We speculate that the primary peak represents the putative M31 spheroid while the more metal-poor population could have originated in a disrupted M31 dwarf satellite galaxy.

5. An examination of the global properties of RR Lyraes in the Andromeda system reveals that, with few exceptions, M31 and its satellite galaxies contain Oosterhoff type I RR Lyraes. This is likely due to the fact that the mean metal abundance of the M31 halo is more representative of Oosterhoff I Galactic globular clusters than of Oosterhoff type II clusters. Needless to say, the mere fact that all of these systems contain RR Lyraes suggests that their earliest epoch of star formation occurred at approximately the same time.

## ACKNOWLEDGMENTS

This work has made use of the IAC-STAR Synthetic CMD computation code. IAC-STAR is supported and maintained by the computer division of the Instituto de Astrofísica de Canarias. We are grateful to the anonymous referee whose comments improved the clarity and quality of this manuscript. We also thank Stéphane Courteau for making available the M31 surface brightness profiles from Courteau et al. (2011). We acknowledge support from NASA through grant AR-12153.01-A from the Space Telescope Science Institute, which is operated by the Association of Universities for Research in Astronomy, Inc., for NASA under contract NAS5-26555.

## REFERENCES

- Alcock, C. et al. 2000, AJ, 119, 2194
- Alonso-García, J., Mateo, M., & Worthey, G. 2004, AJ, 127, 868
- Aparicio, A., & Gallart, C. 2004, AJ, 128, 1465
- Bernard, E. J., Ferguson, A. M. N., Barker, M. K., Hidalgo, S. L., Ibata, R. A., Irwin, M. J., Lewis, G. F., McConnachie, A. W., Monelli, M., & Chapman, S. C. 2012, MNRAS, in press
- Brown, T. M., Ferguson, H. C., Smith, E., Kimble, R. A., Sweigart, A. V., Renzini, A., & Rich, R. M. 2004, AJ, 127, 2738
- Brown, T. M. et al. ApJ, 685, L121
- Chaboyer, B. 1999, in Post-Hipparcos Cosmic Candles, ASSL, Vol. 237, edited by A. Heck and F. Caputo (Dordrecht: Kluwer Academic Publishers) p.111
- Choi, P. I., Guhathakurta, P., & Johnston, K. V. 2002, AJ, 124, 310
- Clementini, G. 2010, in Variable Stars, The Galactic Halo, and Galaxy Formation, edited by C. Sterken, N. Samus, and L. Szabados, (Sternberg Astronomical Institute: Moscow State University) p. 107
- Clement, C. M. & Rowe, J. 2000, AJ, 120, 2579
- Coelho, P., Mendes de Oliveira, C., & Cid Fernandes, R. 2009, MNRAS, 396, 624

- Corbin, M. R., O’Neil, E., & Rieke, M. J. 2001, AJ, 121, 2549
- Courteau, S., Widrow, L. M., McDonald, M., Guhathakurta, P., Gilbert, K. M., Zhu, Y., Beaton, R. L., & Majewski, S. R. 2011, ApJ, 739, 20
- de Vaucouleurs G., de Vaucouleurs A., Corwin H. G., Jr., Buta R. J., Paturel G., Fouqué P., 1991, Third Reference Catalogue of Bright Galaxies (New York: Springer)
- Fiorentino, G., Monachesi, A., Trager, S. C., Lauer, T. R., Saha, A., Mighell, K. J., Freedman, W., Dressler, A., Grillmair, C., & Tolstoy, E. 2010, ApJ, 708, 817
- Fiorentino, G., Contreras Ramos, R., Tolstoy, E., Clementini, G., & Saha, A. 2012, A&A, in press
- Ford H. C., Jacoby G. H., Jenner D. C., 1978, ApJ, 223, 94
- Freedman, W. L. 1992, AJ, 104, 1349
- Freedman, W. L., & Madore, B. F. 1990, ApJ, 365, 186
- Gilbert, K. M., Font, A. S., Johnston, K. V., & Guhathakurta, P. 2009, ApJ, 701, 776
- Grebel, E. K., Gallagher, J. S. III, & Harbeck, D. 2003, AJ, 125, 1926
- Grillmair, C. J., et al. 1996, AJ, 112, 1975
- Guldenschuh, K. A., et al. 2005, PASP, 117, 721
- Harris, W. E., 1996, AJ, 112, 1487
- Impey C. D., Wynn-Williams C. G., Becklin E. E., 1986, ApJ, 309, 572
- Irwin, M. J., Ferguson, A. M. N., Ibata, R. A., Lewis, G. F., & Tanvir, N. R. 2005, ApJL, 628, L105
- Jeffery, E. J., Smith, E., Brown, T. M., Sweigart, A. V., Kalirai, J., Ferguson, H. C., Guhathakurta, P., Renzini, A., & Rich, R. M. 2011, AJ, 141, 171
- Jensen, J. B., Tonry, J. L., Barris, B. J., Thompson, R. I., Liu, M. C., Rieke, M. J., Ajhar, E. A., & Blakeslee, J. P. 2003, ApJ, 583, 712
- Kalirai, J. S. et al. 2006, ApJ, 648, 389
- Koch, A., & Grebel, E. K. 2006, 131, 1405
- Kunder, A., Chaboyer, B., & Layden, A. C. 2010, AJ, 139, 415
- Lauer, T. R., Faber, S. M., Ajhar, E. A., Grillmair, C. J., & Scowen, P. A. 1998, AJ, 116, 2263
- Martin, N. F. et al. 2006, MNRAS, 371, 1983
- McConnachie, A. W., Irwin, M. J., Ferguson, A. M. N., Ibata, R. A., Lewis, G. F., & Tanvir, N. 2005, MNRAS, 356, 979
- McConnachie, A. W. et al. 2009, Nature, 461, 66
- Monachesi, A., Trager, S. C., Lauer, T. R., Freedman, W., Dressler, A., Grillmair, C., & Mighell, K. J. 2011, ApJ, 727, 55
- Monachesi, A., Trager, S. C., Lauer, T. R., Hidalgo, S. L., Freedman, W., Dressler, A., Grillmair, C., & Mighell, K. J. 2012, ApJ, 745, 97
- Pritchett, C. J. & van den Bergh, S. 1987, ApJ, 316, 517
- Pritchett, C. J. & van den Bergh, S. 1994, AJ, 107, 1730
- Reiss, A., & Mack, J. 2004, ISR-ACS 2004-06
- Rose, J. 1985, AJ, 90, 1927
- Rose, J. A., Arimoto, N., Caldwell, N., Schiavon, R. P., Vazdekis, A., & Yamada, Y. 2005, AJ, 129, 712
- Rudenko, P., Worthey, G., Mateo, M. 2009, AJ, 138, 1985
- Salaris, M., Cassisi, S. 2005, Evolution of Stars and Stellar Populations (Chichester: Wiley)
- Sarajedini, A., & Jablonka, P. 2005, AJ, 130, 1627
- Sarajedini, A., Barker, M., Geisler, D., Harding, P., Schommer, R. 2006, AJ, 132, 1361
- Sarajedini, A., Mancone, C., Lauer, T. R., Dressler, A., Freedman, W., Trager, S. C. Grillmair, C., & Mighell, K. J. 2009, AJ, 138, 184 (S09)
- Schlegel D. J., Finkbeiner D. P., Davis M., 1998, ApJ, 500, 525
- Sirianni, M. et al. 2005, PASP, 117, 1049
- Smith, H. A. 1995, RR Lyraes, Cambridge Astrophysics Series, Vol. 27 (Cambridge, UK)
- Stetson, P. B. 1987, PASP, 99, 191
- Stetson, P. B. 1994, PASP, 106, 250
- Suntzeff, N. B., Kinman, T. D., Kraft, R. P., 1991, ApJ, 367, 528
- Tammann, G. A., Sandage, A., Reindl, B., 2003, A&A, 404, 423
- Tonry, J. L., Dressler, A., Blakeslee, J. P., Ajhar, E. A., Fletcher, A. B., Luppino, G. A., Metzger, M. R., & Moore, C. B. 2001, ApJ, 546, 681
- Trager, S. C., Faber, S. M., Worthey, G., & Gonzalez, J. J. 2000, AJ, 120, 165
- Worthey, G. 2004, AJ, 128, 2826
- Yang, S. -C., Sarajedini, A., Holtzman, J. A., & Garnett, D. R. 2010, ApJ, 724, 799
- Yang, S. -C. & Sarajedini, A. 2012, MNRAS, 419, 1362

This paper has been typeset from a TeX/ L<sup>A</sup>T<sub>E</sub>X file prepared by the author.